# UNDER BALLAST MATS FOR RAILWAY INFRASTRUCTURE – A NORTH AMERICAN APPROACH TO COMPONENT CHARACTERIZATION

BY

ARTHUR DE OLIVEIRA LIMA

THESIS

Submitted in partial fulfillment of the requirements
for the degree of Master of Science in Civil Engineering
in the Graduate College of the
University of Illinois at Urbana-Champaign, 2017

Urbana, Illinois

Master's Committee:

Professor Erol Tutumluer, Adviser
Mr. J. Riley Edwards
Mr. Marcus S. Dersch

## ABSTRACT

Railroads continually look for ways to extend the life of their track infrastructure and its components given poor track performance can lead to reduced transportation efficiencies. As such, under ballast mat (UBM) applications have seen growth in the North American (N.A.) freight railroad transportation market. However, current standard procedures quantifying the UBM's properties and performance are provided solely by the German DIN 45673 standard tailored to European Mainline freight and passenger service. This lack of domestic testing procedures tailored to N.A. heavy haul freight lines provides challenges in implementing representative procedures to test materials where the UBMs will be exposed to higher axle loads. To understand how changes to the current procedures may affect the performance of UBM components, laboratory experiments were developed and conducted. Loading magnitudes, loading procedures, support conditions and testing setups were varied during multiple experiments. Additionally, an assessment of the capability of UBMs to increase the allowed track structure deflection under loading (i.e. reduce track stiffness) was also conducted. Results steaming from this work are ultimately intended to provide support to the development of representative characterization procedures and recommended practices for UBMs intended for use in the N.A. market.

**ACKNOWLEDGEMENTS**

Many people have contributed significantly to the realization of both my graduate studies and this thesis work. Without each and every one of them my graduate experience would not have been as enjoyable, nor would the content of this document be as meaningful.

I would not be here without the unconditional support from my family. Thank you to my parents for raising me to be person I am today and teaching me the importance of education, to my brother for always being my best friend and a person I can look up to, and to my little sister for bringing so much love and joy to our lives. Thank you also to my girlfriend for your love and unwavering support every step of the way, both here and 5,200 miles away.

I would like to extend my immense gratitude to Marcus Dersch and Riley Edwards for allowing me the opportunity to find a passion in railway engineering. Their mentorship has been, and will always to be, invaluable in my development as an engineering professional and as an individual. Thanks are due to Professor Erol Tutumluer for his guidance and support throughout this research. The assistance given by Yu Qian and Matthew Csenge also deserves my appreciation. Thank you also to Arkaprabha Ghosh who took the first steps in the investigation of this topic before my arrival and helped me through my first semester. To Professor Chris Barkan, Tyler Dick and Conrad Ruppert, thank you for sharing your immense knowledge in and out of the classroom. Special thanks are also due to RailTEC program coordinators Emma Ehrenhart, L.B Frye and Angie Stanford for making our lives a little easier. Thank you also to Progress Rail Services for their financial support of this research project and my graduate studies.

I am indebted to many fellow students, especially those with whom I have shared work space in B118. Thank you for making it an enjoyable space to spend long days (and nights). The ability to quickly find answers to research (and non-research) questions by simply turning and starting a discussion has been an extremely valuable asset. Your input and feedback throughout discussions and presentations have helped guide and shape the work compiled in this thesis. Special thanks to members of the infrastructure research group with whom many days were spent in the laboratory, in conferences or in the

field.  Also, the help from multiple undergraduate research assistants is much appreciated, this work would not have been possible without their hard work.

*To my family,*

*"Ando devagar*

*Porque já tive pressa*

*E levo esse sorriso*

*Porque já chorei demais*

*Cada um de nós compõe a sua história*

*Cada ser em si*

*Carrega o dom de ser capaz*

*E ser feliz"*

*– Almir Sater & Renato Teixeira "Tocando em Frente"*

**TABLE OF CONTENTS**

# CHAPTER 1: INTRODUCTION

## 1.1 Introduction

The track structure serves two primary purposes: supporting the loads from rail cars and locomotives, and guiding their movements (Hay, 1982). It serves as an elastic load-distributing structure consisting of layers to distribute the highly concentrated wheel-rail interface loads over gradually larger surface areas resulting in stresses that can be supported by the consecutive supporting layer (i.e. rail to rail pad/tie plate to crosstie to ballast to sub-ballast to subgrade).

A common cross section of a track structure (Figure 1.1) consists of the rail supported by crossties (known internationally as "sleepers") and fasteners that are responsible for maintaining the fixed distance between the parallel rails (i.e. the gauge). Crossties rest on a layer of aggregate referred to as the ballast which in turn transmits the stresses to either the soil subgrade or a supporting structure (e.g. bridge deck).

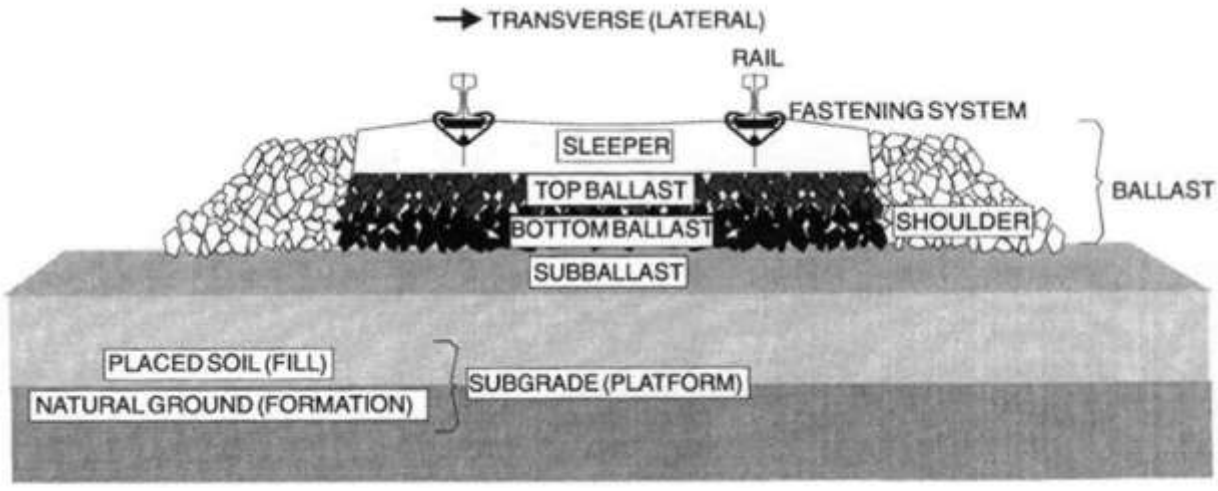


**Figure 1.1 Characteristic ballasted track cross-section (Selig and Waters, 1994)**

In addition to load bearing characteristics, the ballast layer is of paramount importance to the provision of proper drainage through the track structure allowing water to quickly flow away from the

track center protecting the underlying layers (Selig and Waters, 1994). Maintenance and renewal expenses related to track ballast amounted for $1.3 billion in 2015, representing more than 11% of the total annual track and property expenditures across North American (N.A.) Class I railroads (Association of American Railroads, 2016). Excessive degradation of the ballast can contribute to track fouling and settlements (Zarembski, 1993; Selig and Waters, 1994; Giannakos, 2010b; Le Pen and Powrie, 2011). Fouling is characterized by both the stiffening of the ballast, which increases the stresses over the track (Giannakos, 2010a), as well as the disruption of proper drainage which may lead to track instability (Roberts et al., 2006). Consequently, this phenomenon may increase impact loading due to the uneven track surface (Giannakos, 2010b; Le Pen and Powrie, 2011). These effects can be further aggravated in regions of abrupt changes in track stiffness (i.e. transition zones) as will be discussed in Chapter 5. Hence, increasing the life of the ballast is of great interest for both safety and economic efficiency purposes.

In the dynamic movement of trains, the interaction between the uneven surfaces from vehicle wheels and the rail, and the irregular vertical geometry of the track, generates impacts that propagate waves through the track structure (Thompson, 2008). The superposition of several of these randomly oriented waves lead to the excitation of vibrations in the substructure and adjacent ground (Thompson, 2008). There are two key concerns in relation to the effects of these excitations in a railroad. The first relates to the transmission of these vibrations from the ground to nearby foundations and building structure (i.e. ground-borne vibrations). These vibrations may be observed as quivering of the structure and noise originating from the vibration of walls and ceilings; a phenomenon also known as reradiated sound (Müller and Möser, 2013). Secondly, the propagation of this disturbances through the track substructure may lead to accelerated ballast wear rates due to friction further contributing to ballast fouling (Selig and Waters, 1994).

The significance of each of these effects varies depending on the track location and use. Ground-borne vibrations that may affect buildings adjacent to the network are the major concern of transit systems

and other sections of track located in populated areas. In contrast, heavy haul freight corridors are typically located in less populated areas making ground-borne vibration secondary to ballast degradation.

Environmental requirements related to noise and vibration disturbances near new and existing rail lines, especially in populated areas, have become consistently stricter (Hanson et al., 2006). To address this issue and further increase the service-life of track components, it is important to reduce the stress state of the entire track structure, including the ballast (Indraratna et al., 2014). This has driven the industry to seek alternatives to mitigate such disturbances. Various researchers have already reported the benefits of introducing resilient components (e.g. under sleeper pads (USPs) and under ballast mats (UBMs)) in the track structure (Esveld, 2001), both to reduce the propagation of vibrations in the track structure (International Union of Railways, 2011; Müller and Möser, 2013) and slow track quality degradation rates (Sasaoka and Davis, 2005; Auersch, 2006; Dahlberg, 2010; Marschnig and Veit, 2011; Nimbalkar et al., 2012; Schilder, 2013; Indraratna et al., 2014; Li and Maal, 2015).

The introduction of these resilient components in the track structure has been shown to be most effective in mitigating frequencies between 30 to 200 Hz (Wilson et al., 1983; Jones and Block, 1996; Müller, 2008) with insertion loss performances of up to ≈ 18 dB at 63Hz. This is the frequency range considered to cause the most human discomfort (Hussein, 2004). Furthermore, frequencies above this threshold attenuate quickly into the adjacent ground and are not generally considered to be problematic.

Meanwhile, in an assessment conducted for the Austrian Federal Railways, Marschnig & Veit (2011) reported that the implementation of USPs increased the time between tamping cycles by at least 100%. Further, Nimbalkar et al. (2012) concluded that the benefits of introducing resilient pads to the track structure were twofold: (i) attenuate impact forces and (ii) reduce the magnitude and duration of impact forces. Additionally, Nimbalkar et al. (2012) demonstrated a higher efficiency of UBMs in reducing impact magnitudes and ballast damage when installed over stiff supports (e.g. stiff subgrade or structure). Similarly, Indraratna et al. (2014) quantified the impacts of the component on the ballast material degradation under drop-hammer impact loads, reporting reduction values between 46.5% and 65.0% for hard and weak support conditions, respectively. Indraratna et al. (2014) also concluded that the

use of resilient pads provided greater benefits in locations of hard support conditions as the hard support promotes higher particle breakage and the weak support acts as an additional energy absorption medium.

## 1.2 Under Ballast Mats

Under ballast mats are pads made from an elastic material (e.g. recycled tire rubber, Ethylene Propylene Diene Monomer (EPDM) rubber, Polyurethane foam, etc.) and installed below the ballast layer of a ballasted track structure or under the concrete slab in a slab track design. The first reference of a resilient layer being installed in railway track known to the author of this thesis dates back the 1970s with the Japanese Railways exploring innovative methods to reduce track stiffness in tunnels and elevated structures in the Shinkansen high-speed rail line (Sato et al., 1974; Sato and Usami, 1976).

European countries and rail agencies have used and/or studied UBMs for many decades for both passenger and freight services (Wettschureck, 1994; Wettschureck, 1997; Wettschureck et al., 1999; Wettschureck et al., 2002; Wettschureck et al., 2003; Sol-Sánchez et al., 2015). Meanwhile, in N.A., Class I freight railroads have primarily deployed UBMs on ballasted bridge decks (concrete or steel) and tunnels with limited research being conducted to date. While the uses for UBMs relating to reduction of noise and vibration are known, applications in freight railroads are mostly limited to the improvement of track transition performance by providing a reduction in track stiffness on the structure, thus reducing impact loading and differential settlements at the bridge abutments (Mademann and Otter, 2013; Li and Maal, 2015; Lima et al., 2017a). In fact, multiple Class I railroads have employed the component for new ballast deck bridge and/or tunnel construction or retrofit projects (Hanson et al., 2006; Nunez, 2014).

## 1.3 Current Standardized Testing Procedures

The development of characterization tests and the validation of component behavior in revenue service is mostly limited to studies conducted in European nations (e.g. Germany) (Dold and Potocan, 2013; Wettschureck and Kurze, 1985; Wettschureck, 1997; Wettschureck, 1994; Wettschureck et al., 2003; Alves Costa et al., 2012; Sol-Sánchez et al., 2015). Despite significant interest and research undertaken

in Europe, published studies investigating the life cycle of UBMs are quite limited. Nevertheless, reports from tests conducted on samples of UBM materials retrieved from revenue service have demonstrated the capability of the component to retain its properties after many years in service (Wettschureck et al., 2002; Dold and Potocan, 2013). Still, most of the research conducted on product life-cycle characterization is part of product development efforts of private-sector suppliers and, as such, the results are not widely available. Further, there are limited research reports investigating the performance and behavior of UBM components under more extreme axle loading conditions, including N.A heavy axle loads (HAL) (Mademann and Otter, 2013).

To date, the German Deutsches Institut für Normung (DIN) 45673-5, titled "Mechanical vibration - Resilient elements used in railway tracks - Part 5: Laboratory test procedures for under-ballast mats" (Deutsches Institut fur Normung, 2010b), (hereafter referred to as DIN), is the only standardized testing procedure available for the determination of UBM mechanical properties. This document provides guidance for the determination of various characteristics of UBM samples, including static, low- and high-frequency bedding modulus, stiffening ratio, and loss factor. Furthermore, it provides testing procedures for the fitness for specific purpose of the material in the form of mechanical fatigue strength, water absorption and resistance, freeze-thaw resistance, and aging resistance.

UBMs intended for vibration mitigation are typically designed and manufactured to achieve a specific insertion loss, ratio of signal levels (i.e. vibration amplitudes) before and after the installation of a filter (i.e. UBM) in units of decibels, depending on the specified operating environment (e.g. freight, passenger, open track, slab track, etc.). This performance parameter is estimated from prediction models relying on inputs from the characteristics of track structure, loading environment, and materials (Wettschureck, 1997; Auersch, 2006; Hanson and Singleton, 2006). Bedding modulus is one such parameter and has great importance in predicting performance levels. A sensitivity analysis has shown insertion loss predictions to vary on average by between 0.05-0.06 dB/% change in bedding modulus input. Thus, a proper understanding and use of this input property is essential for an accurate prediction of revenue-service track performance.

Hence, the growing interest in N.A. for UBMs has established a demand for the development of uniform testing procedures that can be representative of freight railroad loading environments. Conversely, loading magnitudes in transit applications are less, thus research findings from European studies can be reasonably applied to understand the behavior of UBMs in N.A. transit applications (Vuchic, 2007).

## 1.4 Objectives

The main objectives of this work are to:

- Investigate the effects of increased load magnitude (i.e. N.A. HAL) to currently-available standardized UBM characterization test results;
- Quantify critical test parameter's (e.g. support, sample condition, etc.) influence on the resulting UBM performance metrics;
- Explore alternative test setup(s) to facilitate testing of UBM's fatigue performance;
- Assess benefits of UBMs to mitigate ballast degradation at transition zones.

## 1.5 Thesis Outline

This thesis is divided into six chapters including this introduction. The following paragraphs provide a brief description of the overall scope of each chapter.

Chapter 2 provides a summary of the equipment and basic testing procedures used or referenced in the subsequent chapters. Detailed descriptions of modifications made to standard test equipment are provided along with explanations of design considerations. Further, descriptions of static bedding modulus, explanations of loading magnitudes derived, and fatigue testing procedures are given.

Chapter 3 describes laboratory experiments aimed at investigating the effects of varying testing parameters (i.e. support conditions, loading procedures, and sample conditioning) to the UBM's bedding modulus. Based on the results obtained, a prediction model found in literature is used to quantify the

effect on insertion loss estimations due to differences in bedding modulus input values obtained from tests conducted with different support conditions.

Chapter 4 presents results from mechanical fatigue tests conducted using two different test setups, the “standard” being a ballast box and a proposed alternative being a geometric ballast plate, and two loading conditions: European mainline and N.A. HAL. Results from the two tests are compared to investigate the effectiveness of the new proposed test setup. Additionally, ballast degradation trends are monitored during ballast box tests to provide insights into the impacts of increased loading conditions (i.e. European vs N.A.) on ballast life.

Chapter 5 presents vertical transient deformation amplitude results from tests conducted with and without an UBM installed in the ballast box. It provides insights into the ability of UBMs to reduce stiffness and increase transient deformations at rigid structures to mitigate accelerated degradation rates commonly observed at transition zones.

Lastly, Chapter 6 summarizes all findings presented in this thesis, provides recommendations stemming from the results obtained, and presents ideas for future work.

## CHAPTER 2: LABORATORY EXPERIMENTATION

This thesis presents results from laboratory experiments designed to provide insight into the behavior of UBM samples installed in revenue service conditions. Laboratory experimentation procedures to test/monitor various characteristics and performance criteria of the UBM samples were either adopted (in full or in part) from established criteria or developed internally. As discussed in Chapter 1, to date, UBM laboratory testing criteria have primarily been developed in Europe for the European loading environment. Inevitably, evaluation of the current test procedures was necessary to ensure they represent N.A. revenue service operating conditions which can have loads 61%[1] higher than Europe.

This chapter is divided into sections describing the following elements associated with the testing equipment and procedures employed throughout this research effort and described in this thesis:

- Testing Equipment
    - Pulsating Load Testing Machine (Load Frame)
    - New ballast box design developed by UIUC researchers
    - Geometric ballast plate adopted from Europe's EN 16730:2016
- Testing Procedures
    - Static bedding modulus
        - Definition
        - Equation
        - Loading
    - Mechanical fatigue
        - Loading cycles
        - Loading conditions

[1] Assuming a 49.6-kip (220.6 kN) European axle load and 80-kip (355.9 kN) North American heavy axle load

## 2.1 Testing Equipment

### 2.1.1 *Pulsating Load Testing Machine*

All tests described in this thesis were conducted using the Pulsating Load Testing Machine (PLTM) frame at the Research and Innovation Laboratory (RAIL) in the Harry Schnabel Jr. Geotechnical Laboratory at the University of Illinois at Urbana-Champaign (UIUC). The PLTM, as configured for this experimentation, consists of a 55,000-lb (250-kN) vertical actuator used to apply load during each experiment.

An MTS FlexTest 100 controller was used to control the hydraulic loads applied. All tests were executed in force-control using the MultiPurpose TestWare software (Figure 2.1). This system also monitors and collects data from the actuator's load cell and linear variable differential transformer (LVDT), and from the auxiliary linear potentiometers that are deployed.

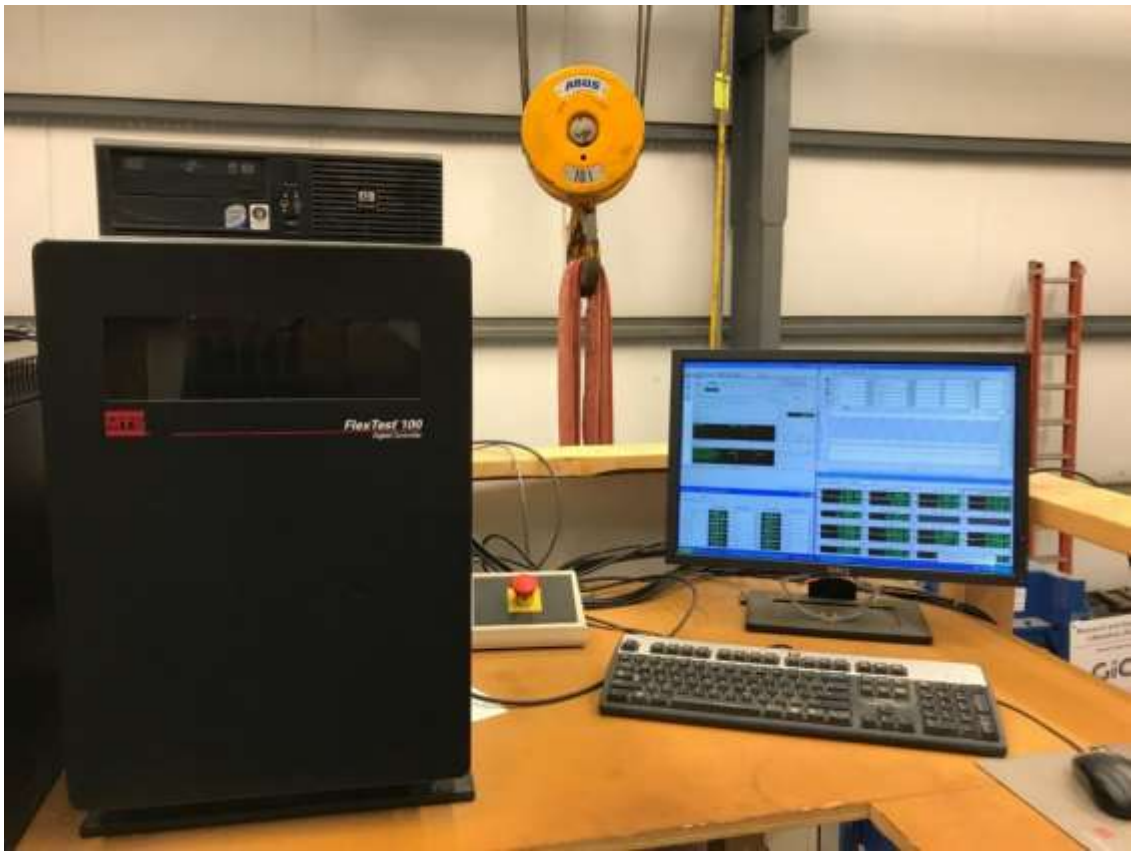


**Figure 2.1 MTS Control System used to control the PLTM actuators**

In the PLTM configuration used in this study, four (4) auxiliary linear potentiometers were used to quantify loading plate vertical displacements; rather than using the displacements recorded within the actuator's LVDT to eliminate non-specimen displacements. The model of potentiometers used has a maximum stroke of 1.18 in. (30 mm) and is accurate to ± 0.001 in. (0.025 mm). Potentiometers were located on each corner of the loading plate, which was attached to the actuator (Figure 2.2). This arrangement exceeded the number of displacement gauges (three) specified by the DIN 45673-5 and can account for any undesirable plate rotation during the tests. To ensure no movement from the lower portion of the setup – especially in dynamic tests – two steel tie-down bars were attached to threaded rods fixed to the floor of the frame (Figure 2.2).

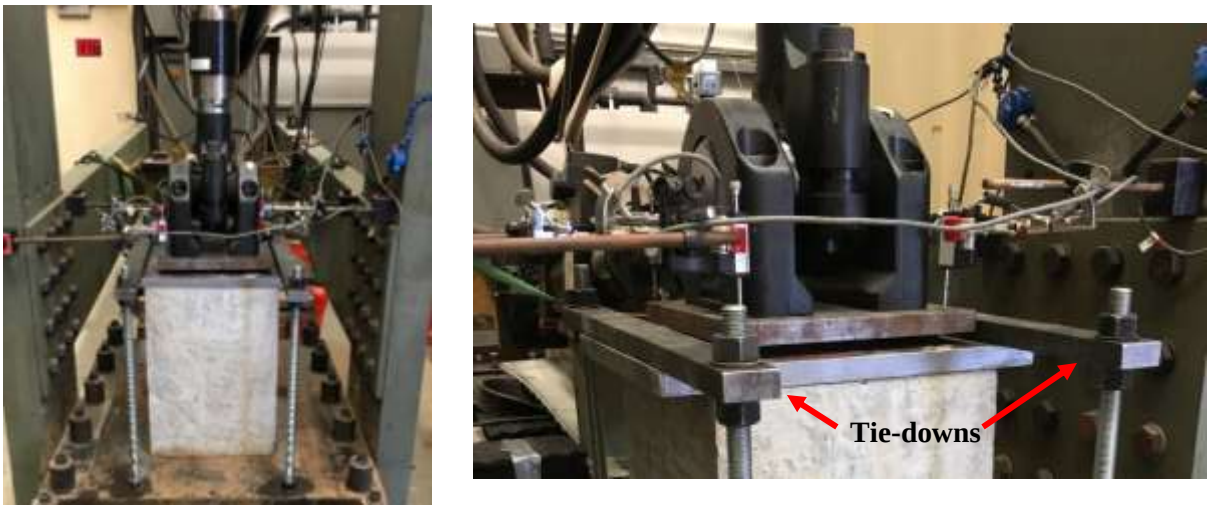


**Figure 2.2 PLTM setup for testing of UBM samples (left) also showing steel plates; (right) detail of potentiometer arrangement.**

### 2.1.2 *UIUC Ballast Box*

A ballast box design for conducting fatigue tests of UBMs is provided in the DIN 45673-5 described in Chapter 1. The design consists of a 39.4 in. by 39.4 in. (100 cm by 100 cm) box capable of accommodating a ballast layer of 11.8 in. (30 cm) thickness. Load is applied to the top of the ballast layer

through a 23.6 in. (60 cm) diameter circular loading plate. However, the adoption of this design presented challenges given the PLTM frame could not house a box of such dimensions. Therefore, the ballast box and loading plate were scaled with the intent to maintain most of the considerations of the original design. Some of the original design considerations known to the authors are listed below and a schematic drawing presented in Figure 2.3 (Stahl, 2016):

1. The circular loading plate area (≈ 438.2 $in^2$ or 2,827 $cm^2$) corresponds to the support area under one rail seat of the German B70 crosstie;
2. The box dimension (39.4 in. or 100 cm sides) allows for a load distribution angle of 45° and for the joint between UBMs to be tested;
3. Applied loads correspond to the rail seat load under a 49.6-kip (22.5-tonne) axle with dynamic impact factor considered.

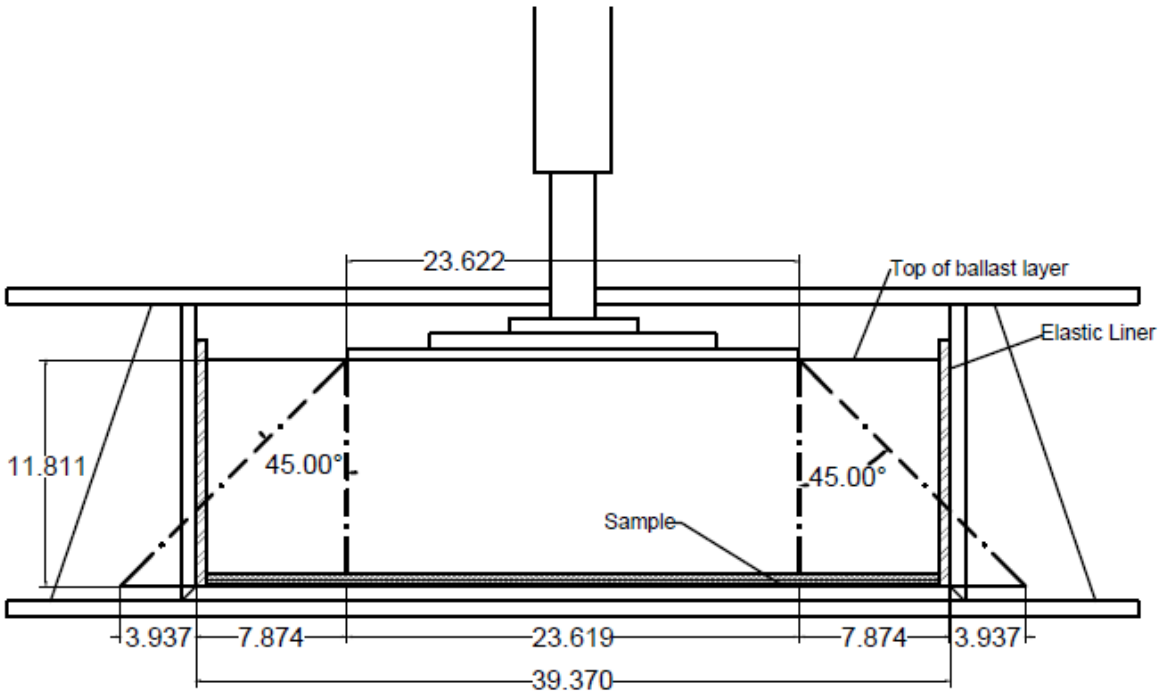


**Figure 2.3 Original DIN ballast box design dimensions and assumptions (dimensions in inches) (Stahl, 2016)**

Some aspects of the original design were preserved, notably ballast layer thickness, and pressures at the tie/ballast and ballast/UBM interfaces. Hence, the newly designed apparatus consisted of a ballast box of 28 in. by 28 in. (71 cm by 71 cm) sides and 14 in. (35.6 cm) depth supporting a full 12-in. (30.5-cm) thick ballast layer while capable of accommodating the thickest UBM sample available to the researchers at this time, and a 12-in. (30.5-cm) diameter loading plate. Additionally, the new box was designed with one removable sidewall for ease of construction and disassembly of the setup. This was particularly important to facilitate the collection of ballast upon completion of tests with minimal loss of material.

As specified within the DIN 45673-5, an elastic liner (Figure 2.3) is required to provide elasticity along the horizontal plane to the ballast layer and better simulate particle confinement experienced in the field. One-quarter inch (6.35 mm) thick neoprene sheets were placed along the sidewalls for this purpose in this system. Figures 2.4 and 2.5 show the UIUC ballast box and loading plate used in experiments presented in Chapters 4 and 5.

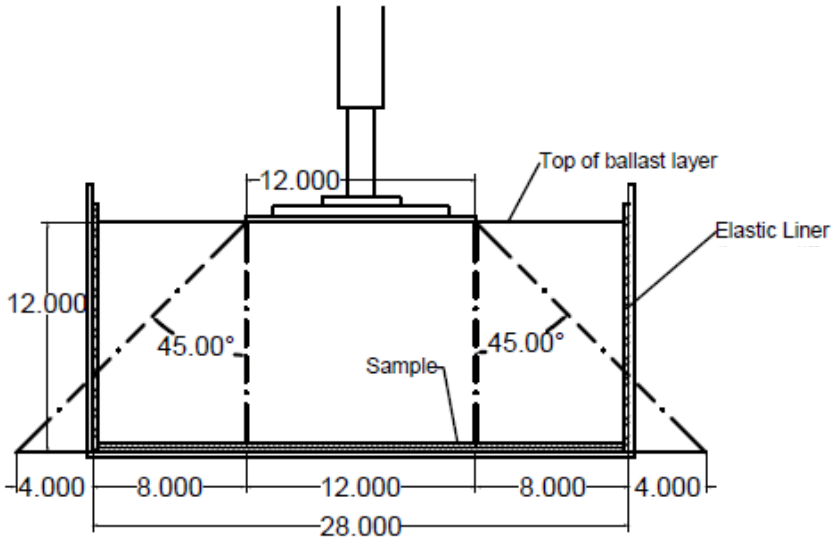


**Figure 2.4 UIUC ballast box design dimensions and assumptions (dimensions in inches)**


**Figure 2.5 Profile view through open sidewall of the UIUC ballast box (demonstration only)**

### 2.1.3 *The Geometric Ballast Plate*

To reduce variability and increase the repeatability of laboratory testing, researchers sought to adopt a standardized ballast surface for UBM characterization tests; these are described in detail in Chapters 3 and 4. The first apparatus investigated was the German DIN Ballast Plate (Schilder, 2013) (Figure 2.6). The German DIN Ballast Plate is a steel cast block mold based on a representative ballast surface. One primary challenge associated with this plate's use is its lack of symmetry (i.e. the placement and orientation of the samples) which influences test results. Beyond this, the plate is no longer manufactured or available to researchers and testing laboratories.

**Figure 2.6 Plan view of a German DIN Ballast Plate at the Getzner Werkstoffe GmbH headquarters**

The solution adopted to overcome issues with the original ballast plate was the European Geometric Ballast Plate (GBP) standardized testing apparatus (European Committee for Standardization, 2016) (Figure 2.8). The aforementioned concerns drove the development of the GBP by the European community with a primary goal of generating a design to represent the same contact surface area as the original German DIN Ballast Plate (Schilder, 2013) (Figure 2.6). The GBP has a complex surface representing various ballast particles yet has symmetric geometry providing a uniform contact surface independent of specimen orientation (Figure 2.7). The most relevant objective of the GBP with respect to this research is to remove the intrinsic variability due to the heterogeneous nature of ballast particles.

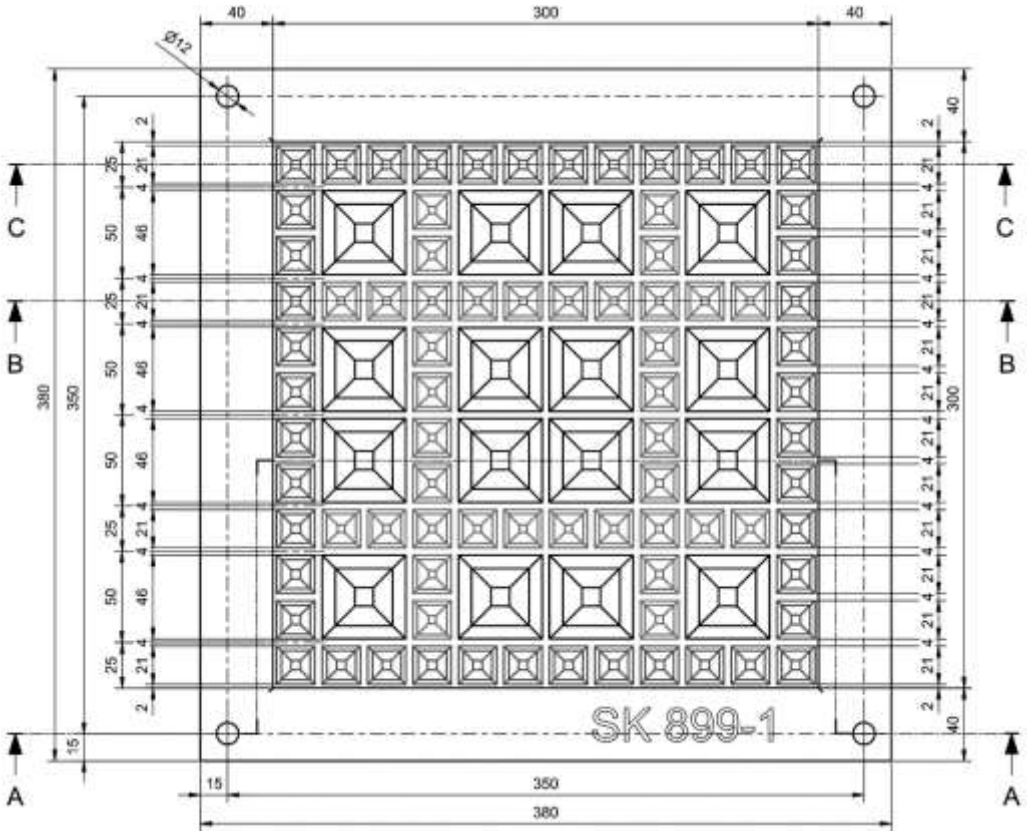


**Figure 2.7 Geometric Ballast Plate schematic drawing (dimensions in mm) (European Committee for Standardization, 2016)**

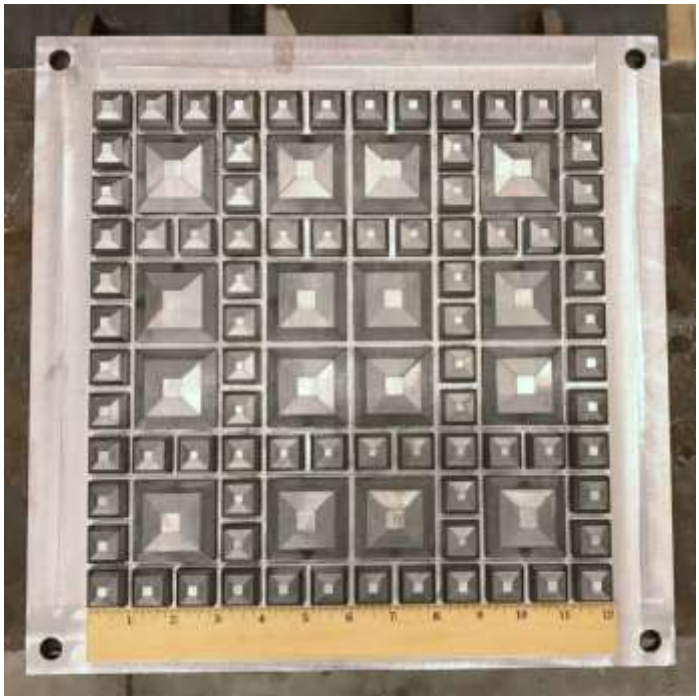

**Figure 2.8 Geometric Ballast Plate manufactured and used at UIUC**

## 2.2 Testing Procedures

### 2.2.1 *Static Bedding Modulus*

Bedding modulus (represented by the symbol "C") is a well-established property used to characterize UBMs as discussed in Chapter 1. The parameter is used as an alternative to stiffness due to its consideration of the tested sample's area and is also believed to better quantify the behavior of rubber-like materials with non-linear stress-strain behavior (Bauman, 2008). The bedding modulus is defined as the amount of force required to displace a unit area by a unit deflection, and is calculated as the tangent, or secant modulus, at a specific stress value in the stress/displacement curve (Equation 2.1).

$$C = \frac{\sigma_2 - \sigma_1}{s_2 - s_1} \tag{2.1}$$

where, $\sigma_1$ = Minimum evaluation stress;

$s_1$ = Displacement at minimum evaluation stress;

$\sigma_2$ = Maximum evaluation stress; and

$s_2$ = Displacement at maximum evaluation stress.

Figure 2.9 shows representative curves for an UBM sample with three evaluation stress ranges depicted; these can be used to quantify representative bedding modulus values for three revenue service loading scenarios.

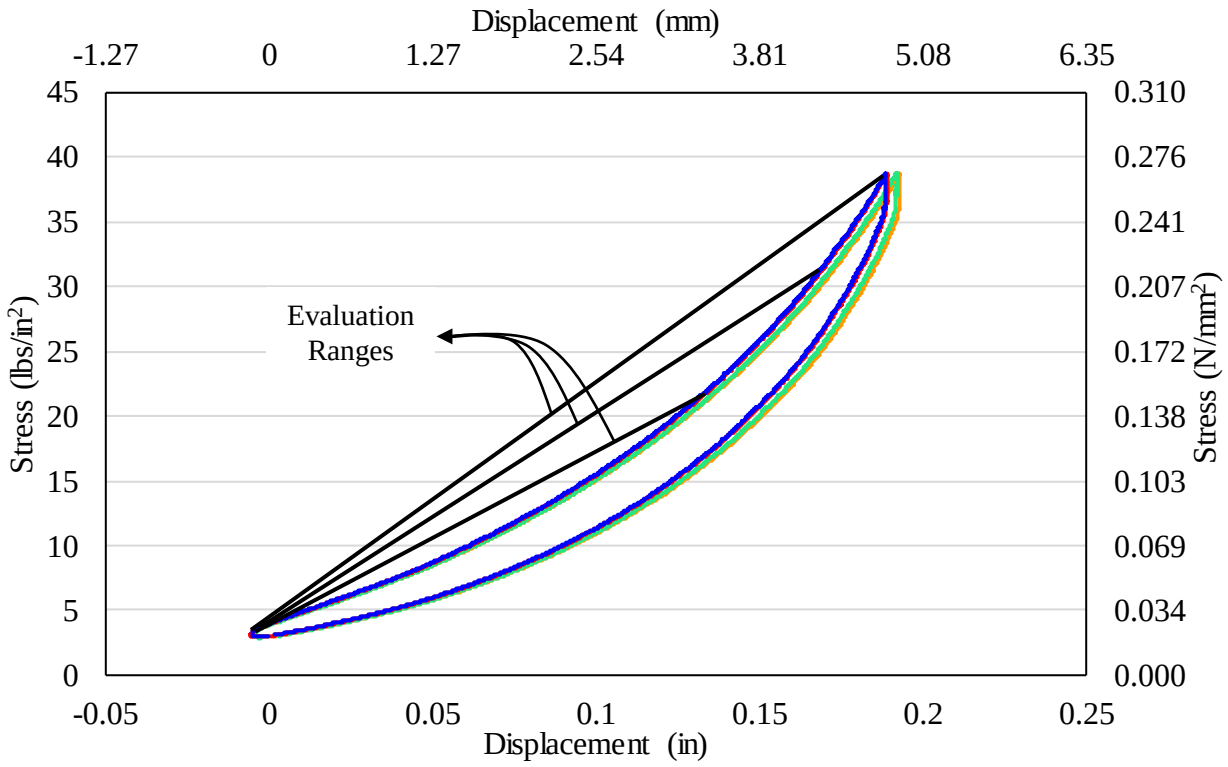


**Figure 2.9 Characteristic hysteresis loop for an UBM sample with four replicate tests showing different bedding modulus evaluation ranges**

The DIN 45673-5 provides information regarding the determination of static bedding modulus ($C_{stat}$) of UBM samples as follows:

- Description of the physical testing setup;
- Test temperature;
- Load ranges (based on typical German axle loads as specified in Part 1 of the same DIN 45673 standard (Deutsches Institut fur Normung, 2010a));
- Load application procedures; and
- Secant modulus equation (Equation 2.1).

The DIN 45673-5 provided the authors with a baseline reference to establish best practices in determining the bedding modulus of UBM samples. Modifications to the procedures were made to both

compare the bedding modulus values under European freight and passenger service loads as well as the N.A. loading environment.

To accurately represent the N.A. loading environment, a new maximum load magnitude was derived. To quantify the maximum load magnitude to be applied to the specimen, the Talbot equation (Talbot, 1920) and Boussinesq formulation (Kerr, 2003) were used to relate axle load to ballast stress. Talbot's formulation was chosen to determine the stress value for a typical axle load as it represented a more conservative scenario. The 95$^{th}$ percentile typical N.A. heavy haul axle load of 80 kips (356 kN) (Van Dyk, 2013), produces a ballast stress of 38 psi (262 kPa) assuming a ballast depth of 12 in. (30.5 cm) below the crosstie. With this stress, and a UBM sample size of 10 in. by 10 in. (25.4 cm by 25.4 cm), the maximum load to be applied in the tests was calculated to be 3.8 kips (16.9 kN).

### 2.2.2 *Mechanical Fatigue*

Mechanical fatigue testing procedures in the DIN 45673-5 comprise of two stages of cyclic loading at incremental load levels (i.e. load levels 1 and 2) and constant frequency in the range of 3 to 5 Hz. Sample temperature should not exceed 104°F (40°C), and the loading frequency is controlled such as to avoid heat build-up in the sample tested. The two test stages apply 10,000,000 and 2,500,000 load cycles, respectively. This results in continuous testing lasting between 29 and 48 days depending on the loading frequency employed.

Consequently, due to the substantial amount of time required to perform the complete test procedure, as well as the fact that the second stage loading produces the greatest amount of damage, it has become common practice by UBM manufacturers to restrict testing to second stage loading (i.e. 2,500,000 cycles), which reduces the testing time by 80%. This protocol still provides an appropriate indication of component performance – especially in cases of relative comparison such as the one presented in this research – as the majority of the damage incurred originates from the higher load magnitudes employed during the second stage of testing. Further, a similar number of cycles is used elsewhere in fatigue testing of resilient components (BS EN 16730, 2016). Hence, this work presents

results of tests performed using both the complete procedure (Chapter 5) and only the second stage of testing (Chapter 4) in the DIN 45673-5.

Both qualitative and quantitative assessments of the UBM performance were performed after/during the tests conducted as directed by the DIN (Deutsches Institut fur Normung, 2010b). Primarily, a qualitative assessment of physical damages incurred to the specimens tested was performed after each of the tests to ensure UBM samples could withstand high contact stresses and friction against ballast particle edges. Additionally, to quantify the relative change in the component's vibration mitigation performance, static bedding modulus values for each sample were determined prior-to and subsequent to the applied fatigue loading as specified in the DIN 45673-5.

Bedding modulus values were determined for specific load ranges for which the component is intended. Table 2.1 presents the evaluation ranges considered for each of the two scenarios investigated. It is worth noting that even though the evaluation ranges employed are individual to each scenario, both samples were loaded to the full load range of the N.A. scenario to maintain consistency of testing and enabling researchers to later evaluate bedding modulus values in additional load scenarios.

**Table 2.1 Bedding modulus evaluation ranges employed**

| Loading Scenario | Evaluation Range [kips (kN)] | | Loading Rate [psi/s (Mpa/s)] | No. of Cycles [Applied/Recorded] |
|---|---|---|---|---|
| | Minimum | Maximum | | |
| European | 0.2 (0.9) | 2.9 (12.9) | 1.45 (0.01) | 3/1 |
| North American* | 0.2 (0.9) | 3.8 (16.9) | 1.45 (0.01) | 3/1 |

* Load range employed for all tests.

*2.2.2.1 Loading Conditions*

To quantify the effects of European and N.A. loads on the fatigue performance of the component, both load scenarios were simulated. For the first scenario, the maximum load was of 22.5 kips (100 kN) as given by the DIN 45673-5. To maintain the same stress level of the DIN 45673-5 (i.e., 51.3 psi or 354 kPa) with the reduced-size loading plate of the UIUC ballast box (described in Section 2.2.2), the DIN

specified load was scaled based on the loading plate area. The resulting load value to be employed during testing was determined as 5.8 kips (25.8 kN).

Next, the equivalent N.A. load was quantified based on the assumption of the 95$^{th}$ percentile nominal N.A. heavy axle load of 80 kips (356 kN) (AREMA 2016) and a back-calculation of the DIN-employed impact factor. The main considerations used by the DIN 45673-5 standard procedure and applied in the impact factor back-calculation are listed below:

- 49.6 kips (22.5 tonnes) European mainline axle load;
- Loading plate area which corresponds to the support area under one rail seat of the German B70 crosstie.

Given these considerations, and the assumption that the crosstie directly below the loading axle supports 50% of the axle load, a dynamic impact factor of 1.8 was calculated and used in the determination of an equivalent load of 36.3 kips (161 kN) for the N.A. scenario. Subsequently, the applied test load was scaled based on the same considerations previously described for the European load scenario due to the reduced loading plate size resulting in an applied load of 9.4 kips (41.6 kN). Table 2.2 presents additional details of both loading scenarios used.

**Table 2.2 Fatigue loading procedures employed**

| Loading Scenario | Load Level | Loading Range [kips (kN)] | | Sinusoidal Frequency [Hz] | No. of Cycles |
|---|---|---|---|---|---|
| | | Minimum | Maximum | | |
| European | Level 1 | 0.4 (1.8) | 4.4 (19.6) | 5 | $10x10^6$ |
| | Level 2 | 0.4 (1.8) | 5.8 (25.8) | 5 | $2.5x10^6$ |
| North American | Level 1 | 0.4 (1.8) | 7.1 (31.6) | 5 | $10x10^6$ |
| | Level 2 | 0.4 (1.8) | 9.4 (41.6) | 5 | $2.5x10^6$ |

## 2.3 Testing Framework Summary

A variety of combinations of the aforementioned testing procedures and setups were employed throughout this thesis. To facilitate the reader's understanding of how these are connected, Figure 2.10 provides a "roadmap" to all tests described in this thesis' chapters.

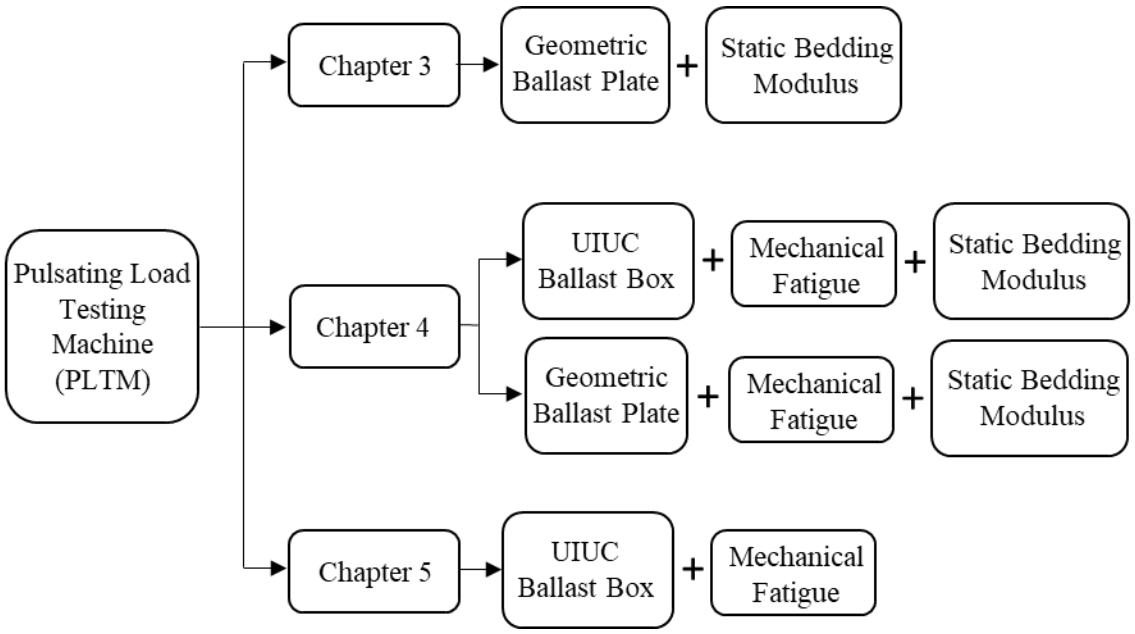


**Figure 2.10 Flow chart summary of testing procedures and equipment described in thesis chapters**

# CHAPTER 3: BEHAVIOR OF UNDER BALLAST MATS UNDER VARYING LOADS AND SUPPORT CONDITIONS[2]

## 3.1 Introduction and Background

Currently, established laboratory testing procedures which quantify bedding modulus use two steel plates to apply loads and simple pre-load conditioning of the sample (Deutsches Institut fur Normung, 2010b); this method is described in detail in Section 2.2.1. It is hypothesized, however, that the bedding modulus value quantified in this manner may not fully represent revenue service conditions and therefore may lead to unrealistic estimations of insertion loss performance. To investigate this hypothesis, experiments were developed to study the effects of varying support conditions, loading procedures, and sample conditioning to the under ballast mat's (UBM) static bedding modulus ($C_{stat}$) values as well as their resulting insertion loss. Insertion loss is a performance metric quantifying the ability of a material to mitigate the transmission of vibrations in railway tracks (Hanson et al., 2006) and its correct estimation is critical to the successful selection of a mitigation strategy as mentioned in Chapter 1.

Moreover, findings from this research (Lima et al., 2017b), described in detail in Chapter 4, suggest that sample load history and rest period have a substantial effect on the UBM stiffness characteristics. A literature review of the mechanical behavior of elastomeric materials under load suggested these to be a result of strain-crystallization effects in the crystalline networks of the rubber (Bauman, 2008; Mars and Fatemi, 2004; Woo and Park, 2011). This necessitates studying UBM's revenue service working range.

[2] Much of Chapter 3 was submitted for consideration for publication in the 2018 Transportation Research Record (TRR): Journal of the Transportation Research Board (TRB).

## 3.2 Methodology

### 3.2.1 *Experimental Setup*

As referenced in Chapter 2, testing was conducted using the Pulsating Load Testing Machine (PLTM) (Section 2.1.1). In this test setup, four (4) potentiometers quantified vertical displacements on each corner of the loading plate (Figure 3.1). Considerations were also made to ensure that the UBM sample was the only component to deform as the concrete block and frame were assumed to be rigid.

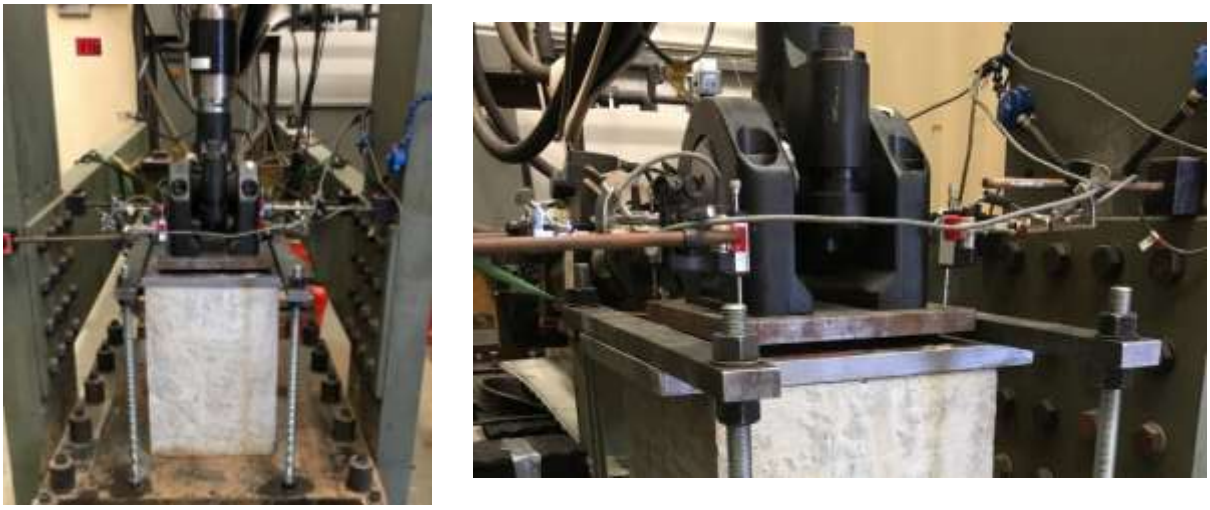

**Figure 3.1 PLTM setup for bedding modulus testing of UBM sample (left) also showing steel plates; (right) detail of potentiometer arrangement.**

### 3.2.2 *Experimental Test Matrix*

An experimental test matrix was developed to investigate the effect of support conditions and loading procedures on bedding modulus quantification. Three UBM designs with varying thicknesses and geometries were subjected to the testing procedures described below. Samples were labeled in sequential order as A, B, and C according to their maximum thicknesses. Table 3.1 presents the general characteristics of the UBM samples tested.

**Table 3.1 Under ballast mat sample characteristics**

| Label | Color | Mat Thickness [in. (mm)] | | Sample Size [in. (mm)] | Construction |
|---|---|---|---|---|---|
| | | Minimum | Maximum | | |
| Type A | Black | 0.197 (5) | 0.394 (10) | 10 (254) | Profiled mat bonded to flat protective layer |
| Type B | | 0.315 (8) | 0.670 (17) | x | |
| Type C | | 0.275 (7) | 0.984 (25) | 10 (254) | |

#### 3.2.2.1 Support condition effects

To quantify how support conditions affect UBM bedding modulus, three support conditions were tested in the laboratory. A baseline value was obtained using the support specified within the DIN, and two additional supports, which better represent the UBM field service conditions, were also tested. As discussed previously, this experimentation was important given that the UBM's bedding modulus is a critical input into the insertion loss prediction models, and slight changes in bedding modulus can influence the predicted performance.

Support conditions were selected with the objective of replicating the field conditions to which the material would be subjected. Hence, a 14x14x28 in. (35.6x35.6x71.1 cm) concrete block support (Figure 3.2a) was used to represent applications on concrete bridge decks, tunnels, or floating slab track. The European GBP (Figure 3.2c), presented in Section 2.1.3, was used as a means to simulate applications in ballasted track (installation on sub-ballast) by representing railroad ballast discrete contact points ballast); please note that the sample orientation changed to ensure the UBM was oriented properly with regards to the GBP (Figure 3.2c). Finally, a steel plate (Figure 3.2b) was adopted as the control setup as recommended within the German DIN 45673-5. For all cases, load was applied using a flat steel plate attached to the actuator head.

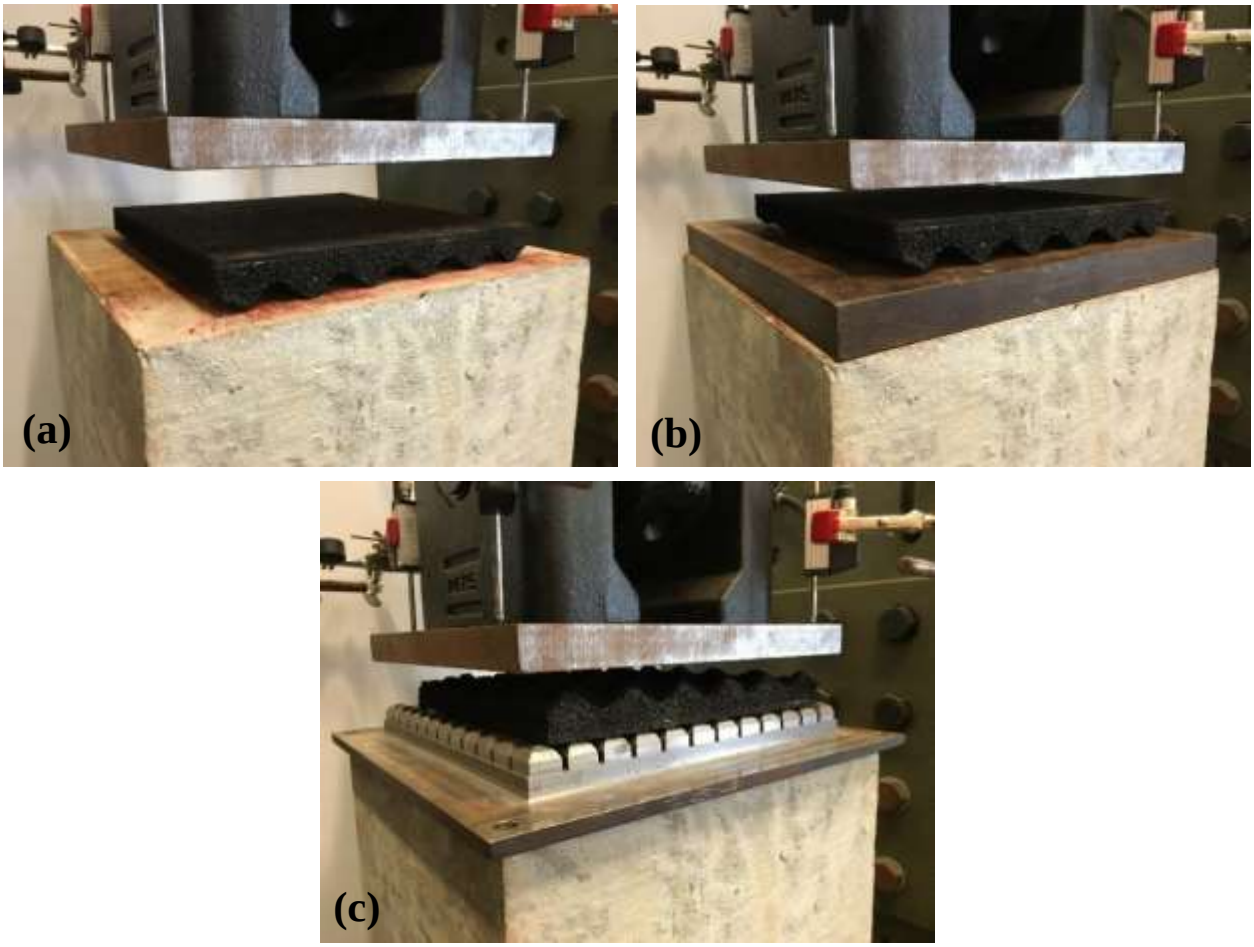


**Figure 3.2 Support conditions used in the experiment: (a) Concrete; (b) Steel; (c) GBP**

#### 3.2.2.2 Traffic pattern effects

To quantify an UBM's stiffening due to loading, three separate test scenarios were developed. The first two scenarios were performed only on Type A samples and were considered to represent the behavior of the other samples in this study while the third testing scenario was performed on all three sample types (Figure 3.3).

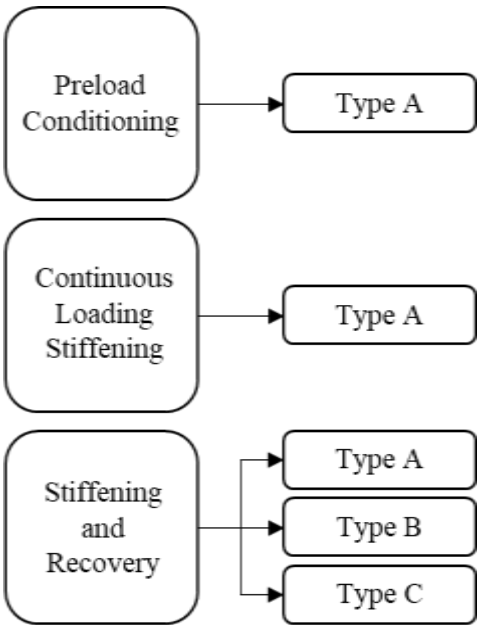


**Figure 3.3 Matrix of loading scenarios and sample types**

First, a loading scenario – Preload Conditioning – was developed to quantify the change in component stiffness due to initial conditioning of the UBM samples during the preload phase of testing (Figure 3.4). This was achieved by observing the changes in bedding modulus, for the same sample, over preload time intervals of 1, 2, 3, 5, 10, 30, 45, 60, and 120 minutes. All samples were allowed a period of unloaded rest for either 2 or 6 hours between preload applications.

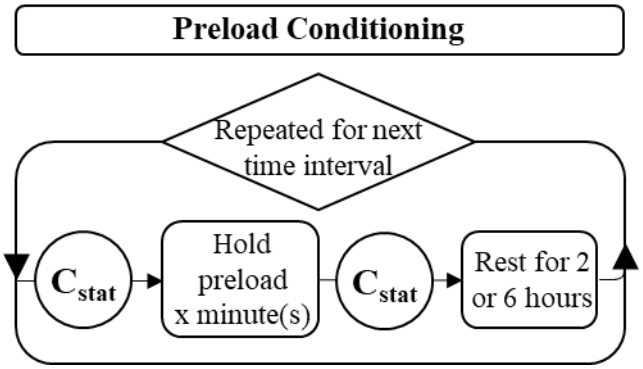


**Figure 3.4 Preload conditioning procedure flowchart**

The second loading scenario – Continuous Loading Stiffening – was developed to quantify the change in component stiffness (i.e. static bedding modulus) due to continuous loading (Figure 3.5). UBM samples were first subjected to a preload and then to cycles of loading at a frequency of 5 Hz. Measurements of static bedding modulus were obtained once every 50 cycles of loading for up to 1,500 cycles. Immediately after the 1,500 cycles were applied, the UBMs were held statically at maximum load for 10 minutes. After, the applied load was reduced to the initial preload level for sample rest during which time bedding modulus values were obtained at incrementally longer intervals of 10, 30, and 120 minutes.

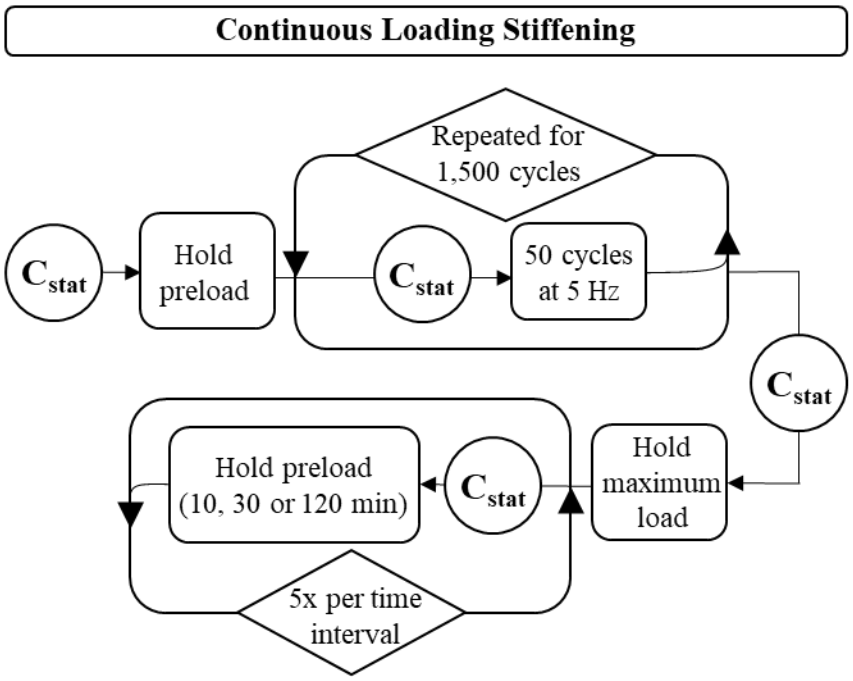


**Figure 3.5 Continuous loading stiffening procedure flowchart**

The final loading scenario – Stiffening and Recovery – was developed to quantify the stiffening and recovery of the UBM samples during representative in-service loading conditions and how this stiffening would affect the bedding modulus of the UBM over time (Figure 3.6). This was achieved by simulating revenue service traffic patterns for a rail transit line. New York City Transit Authority rolling

stock was simulated assuming 32 axles per train consist and headways varying between 3, 5, and 10 minutes. Headways were varied to quantify the effect of traffic density/rest period on UBM bedding modulus.

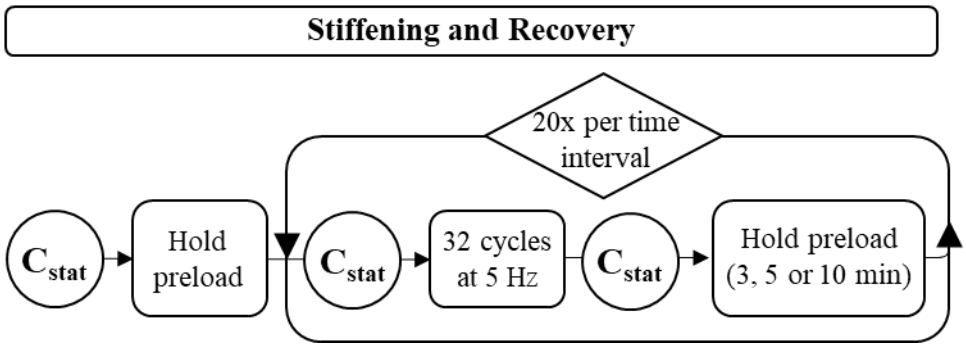


**Figure 3.6 Stiffening and recovery procedure flowchart**

### 3.2.3 *Testing Procedures*

Static bedding modulus measurements for the investigation of support condition effects were performed in accordance with DIN procedures. Three cycles of quasi-static loads within the range of 0.2-3.8 kips (0.9-16.9 kN) were applied to each sample following a continuous loading and unloading rate of 1.45 psi/s (0.01 $N/mm^2/s$) as described in Section 2.2.1. Measurements of force and displacement were obtained for the last complete loading cycle. For the experiments performed in this investigation, four test replicates were conducted to assess the level of variability with the proposed test procedure.

During the investigation of the effect of traffic pattern, test procedures were further modified to allow for more precise capture of the stiffening and recovery effects of traffic. The traffic loading range employed consisted in a preload/minimum load of 0.4 kips (1.8kN) specified by the DIN and maximum load of 3.8 kips (16.9kN) as described in Section 2.2.1. For the determination of the static bedding modulus at each stage, load ranges were held constant but only a single load cycle was performed. Tests were executed this way given the two initial conditioning cycles, recommended by the DIN procedures, could impart changes to the bedding modulus results and thus mask the true effects of traffic loading.

### 3.2.4 *Insertion Loss Prediction Model*

Various models to determine the expected performance of UBMs have been developed (Auersch, 2006; Alves Costa et al., 2012; Wettschureck and Kurze, 1985), one of which was developed by Wettschureck and Kurze (W&K). W&K's model was evaluated using data from previous field investigations available to the researchers. These data were used as inputs to the model to compare the predicted performance to field measurements of insertion loss that were part of the field study. Based on this investigation, W&K's model was found to provide satisfactory results and was chosen for subsequent use.

This theoretical impedance model consists of a unidimensional, single degree-of-freedom representation of the track structure in which three separate impedances are considered. First, the source impedance represents all track components above the level of installation of the UBM, including: ballast, crosstie, rail, fasteners and unsprung wheelset mass. Second, an individual impedance value depicts the UBM (i.e. filter) to be added to the structure. Lastly, the terminal impedance includes characteristics of the support in which the material is to be installed (i.e. either the subgrade or a concrete slab). A schematic representation of the W&K model is presented in Figure 3.7.

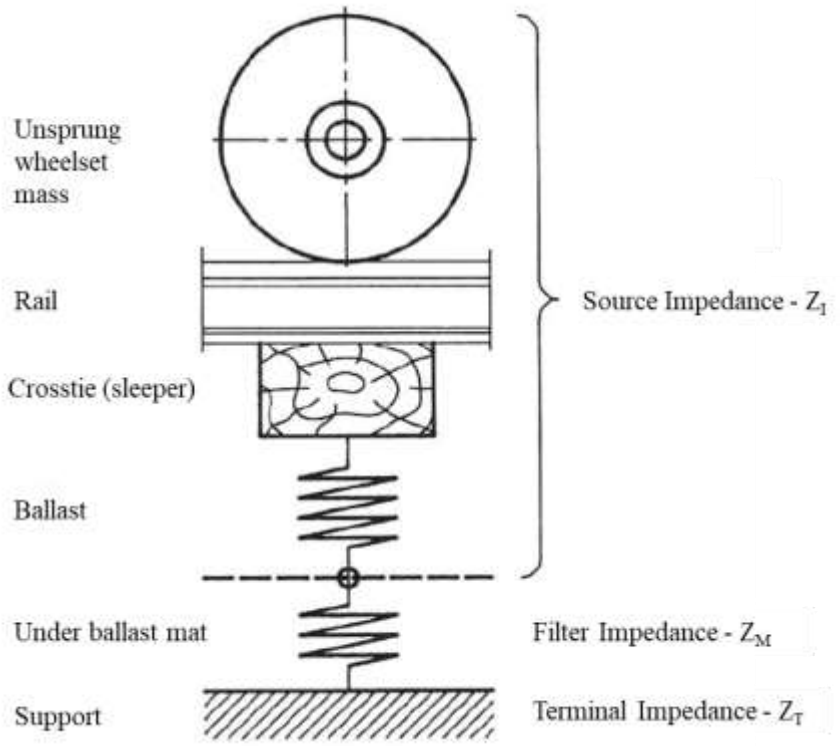


**Figure 3.7 Representation of the insertion loss model by W&K (adapted from Wettschureck and Kurze, 1985)**

Following are the equations derived from the model depicted in Figure 3.7. These equations describe the determination of insertion loss based on all impedance values.

$$\Delta L_e = 20 \log \left| 1 + \frac{\frac{j\omega}{s_M}}{\frac{1}{Z_i}+\frac{1}{Z_a}} \right| dB \tag{3.1}$$

where, $\Delta L_e$ = insertion loss (dB);

$j$ = imaginary unit;

$\omega$ = radian frequency (Rad);

$s_M$ = UBM stiffness (N/m);

$Z_i$ = source impedance; and

$Z_a$ = terminal impedance.

Note that the UBM stiffness $s_M$ in the above is determined using the following equation:

$$s_M = s''_M \times S_w \times (1 + jd_M) \tag{3.2}$$

where, $s''_M$ = dynamic bedding modulus (N/m$^3$);

$Sw$ = effective load transfer area of the ballast-UBM interface (m$^2$); and

$d_M$ = loss factor of the UBM.

It is important to note that the values of static bedding modulus are used as a proxy to compare results within this study – using insertion loss estimations – and are not intended to be used as a real estimation of the component's performance due to its dynamic nature. In this case, static bedding modulus has been employed as a proxy for UBM performance and so input as $s''_M$ in the above equation. Further, the effective load transfer area ($S_w$) employed in Equation 3.2 is determined from Equation 3.3 below described by Wettschureck and Kurze (1985).

$$S_w = 2\left[\left(2ü + \frac{2d'}{\tan\varphi}\right)\left(b_1 + \frac{2d'}{\tan\varphi}\right)\right] \tag{3.3}$$

where, 2ü = Effective support length under each railseat;

$d'$ = ballast thickness above UBM;

$b_1$ = crosstie width; and

$\varphi$ = load distribution angle.

An adapted diagram from W&K's work is presented in Figure 3.8 and depicts all parameters employed in the above equation. In his research, W&K provides proposed values to be input in Equation 3.3. A suggested value of $S_w$, calculated based on those, is derived as 55 in. (1.4 m). However, for the calculations performed in this research, some of the proposed values were not employed as new considerations were adopted. The effective support length ($2ü$) was assumed to be approximately one-

third of the length of a typical N.A concrete crosstie resulting in a value of 39.4 in. (0.9 m). Typical crosstie dimensions also determined the value of $b_1$ to be input as 11 in. (0.27 cm). Ballast thickness above the UBM ($d'$) was chosen to be 12 in. (30 cm), a very typical value found in N.A railroads. Lastly, the load distribution angle $\varphi$ was taken to be 60°, as recommended by W&K (Wettschureck and Kurze, 1985).

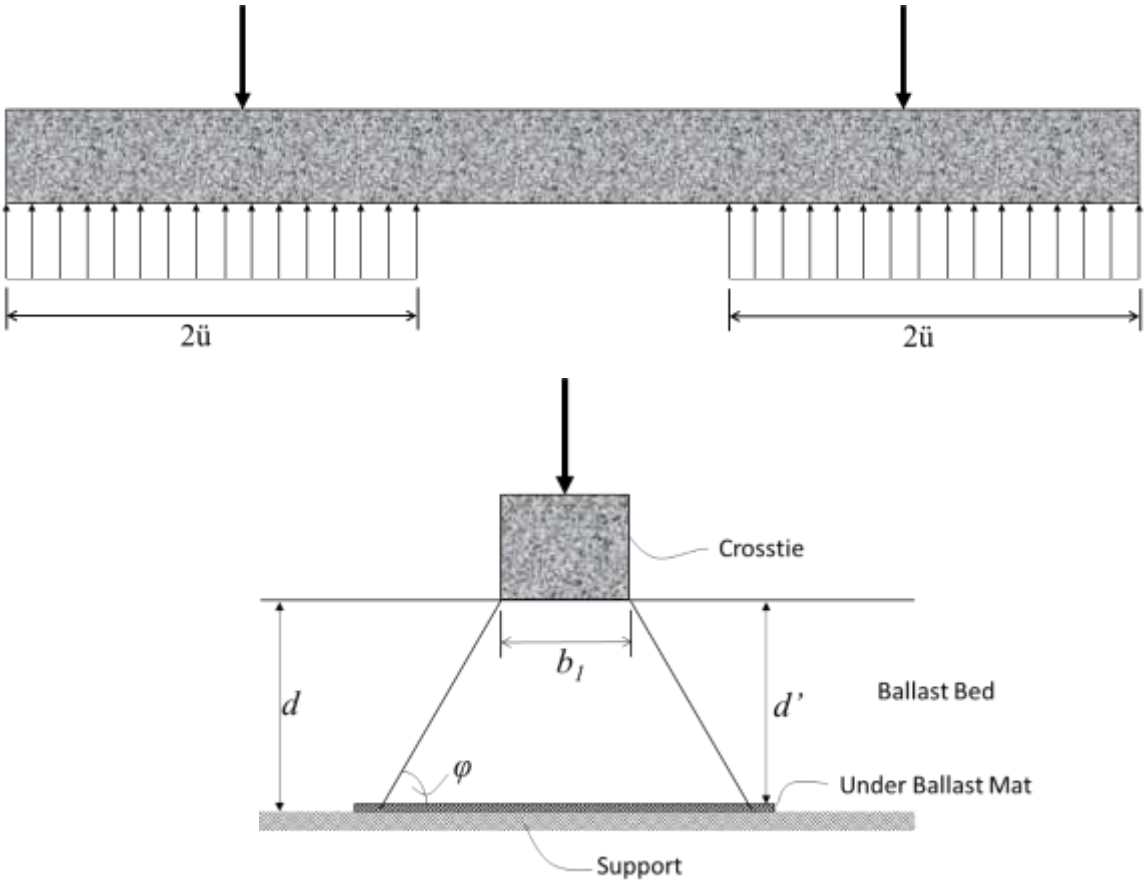


**Figure 3.8 Longitudinal (top) and cross-sectional (bottom) diagrams of variables for the determination of the effective load transfer area $S_w$ (adapted from Wettschureck and Kurze, 1985)**

### 3.3 Results and Discussion

Measurements of displacement from all potentiometers were zeroed based on their initial recorded values and subsequently averaged to obtain the absolute deformation (i.e. UBM displacement). Force

measurements were used to compute the stress using the total area of the specimen being tested. A sample of these results is presented in Figure 3.9, which shows hysteresis loops as overlapping curves for all four replicates of sample Type C tested with the steel support condition.

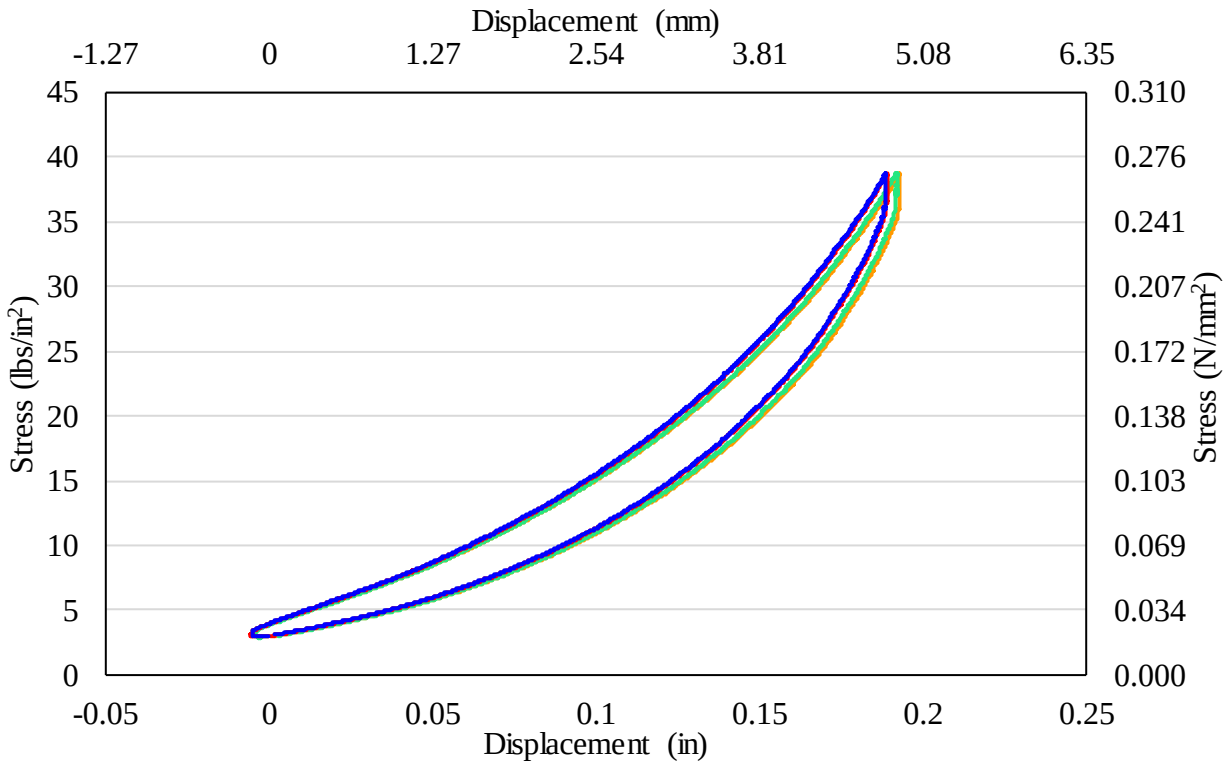


**Figure 3.9 Hysteresis loops for sample Type C with steel support condition**

The hysteretic behavior of the UBM elastic material is clearly shown in Figure 3.9 indicating the occurrence of energy dissipation due to internal friction in the material (T. J. LaClair, 2006). This results in loss of strength in the unloading phase of the test providing lower stress values for a same strain measurement. Energy loss in the system may be represented by the work corresponding to the area engulfed by the loop (Hopkinson and Williams, 1912).

### 3.3.1 *Support Condition Effects*

Based on the values presented in the hysteresis loop, the bedding modulus for each test was calculated as the secant modulus of each loop per Equation 2.1. This process was replicated for all tests performed and a summary of the mean results from all replicates is presented in Figure 3.10.

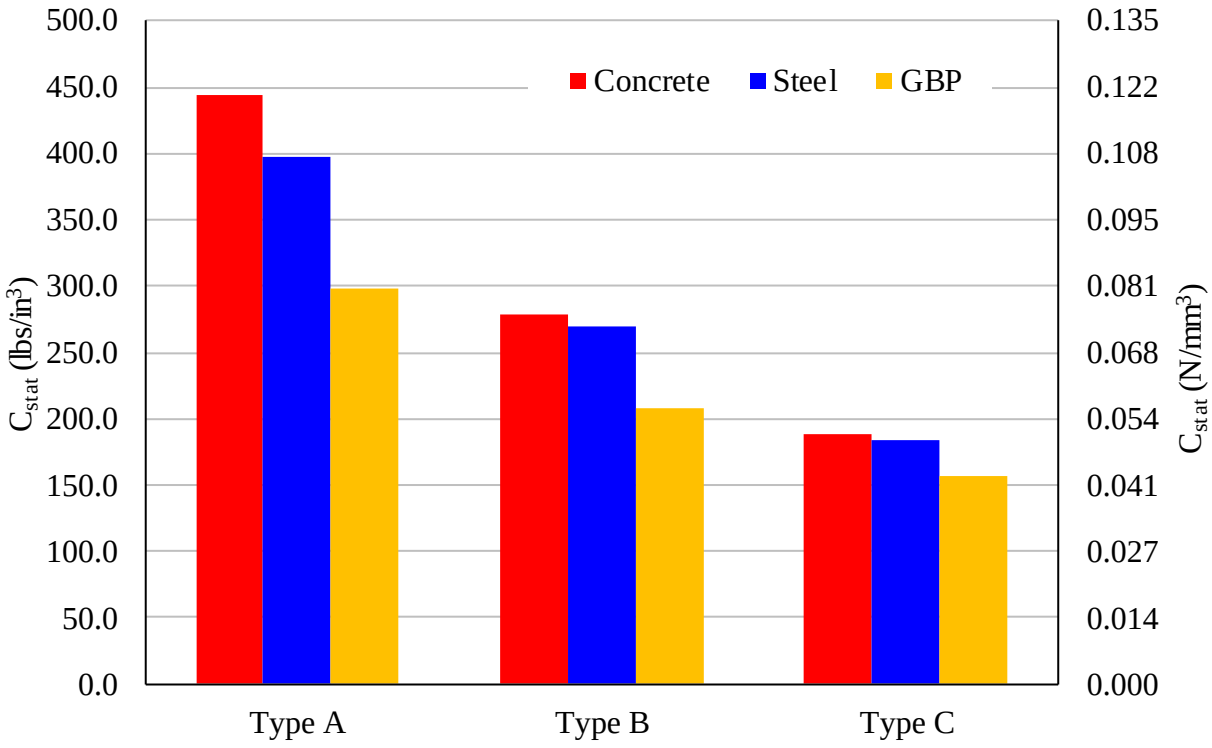


**Figure 3.10 Bedding modulus results for samples tested**

Consistency of the measurements was observed throughout all tests. Measurements of the variability were taken as the maximum absolute percentage deviation from the mean within a single test procedure, and these were found to be 1.7% for steel, 3.8% for concrete, and 2.3% for the GBP in all tests conducted as part of this experimental program. Given the low variability within a given sample and support condition, averages of the replicates were chosen as a reasonable method to present the results.

As can be seen from Figure 3.10, there is a noticeable difference between all support conditions, with a trend of concrete consistently yielding the highest values of bedding modulus, followed by steel,

and lastly by the GBP. Comparatively, concrete and steel provided comparable results, with the GBP yielding slightly lower values. The differences among the samples range from as low as 2.3% for Type C to 11.7% for Type A (Figure 3.10) between concrete and steel supports. One possible reason for such differences could be the effect of frictional forces between the UBM and the concrete surface microstructure. Due to Poisson's effect these frictional forces could induce lateral confinement of the sample imposing additional restrictions to the vertical deformation of the material resulting in reduced deformations for the same applied load.

Further, the GBP support displayed the lowest overall bedding modulus for all support conditions with values up to 33.3% lower than the results from the same tests performed on concrete or steel. This may be explained by the presence of the profiled surface of the plate, providing space for the material to deform, which is not present for either the concrete or steel supports. Nevertheless, statistical analysis conducted with a significance (alpha) level of 0.05 demonstrated all results to be significantly different across support conditions.

### 3.3.2 *Traffic Pattern Effects*

Similarly, bedding modulus values were calculated for each step of the traffic loading pattern simulation procedures for each sample as previously described. Results from the first simulation are presented in Figure 3.11 and demonstrate the effects of preload conditioning time showing that the initial stiffening of the sample occurs at a rate greater than the procedure is capable of detecting, and the continuance of such load over the sample for extended periods of time does not significantly change the sample stiffness. Though similar trends were observed between the two tests conducted with different rest periods between preload applications, a statistical analysis with a significance value of 0.05 concluded that there was statistical difference between the results. This finding is consistent with the results previously described in which the recovery of the sample occurs within the first few minutes of sample unloading.

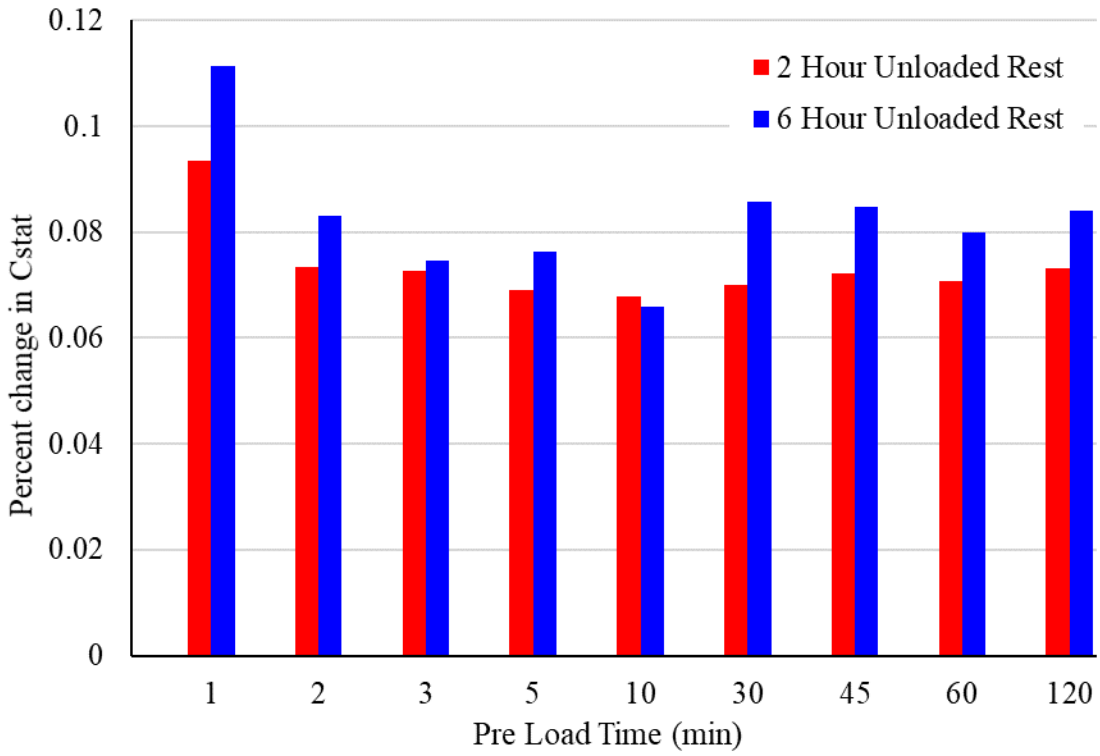


**Figure 3.11 Effects of preload conditioning time results**

Next, results shown in Figure 3.12 and 3.13 for continuous loading stiffening tests demonstrate a consistent increase in bedding modulus values with incremental loading cycles for the four Type A samples tested. A maximum increase of 25% was found after 1,500 cycles of loading plus 10 minutes of constant load. Further, it is possible to observe the rapid development of elastic recovery for all samples after only 10 minutes of rest under preload reaching stiffness values lower than the initial preload conditioning.

It is also worth noting the inflection point, which is present in all curves after approximately 200 minutes of testing. One possible explanation for the inflection point is that there is a change in the net balance between the recovery of the preload rest and the stiffening due to the loading imparted while measuring the sample's static bedding modulus. Moreover, the recovery of samples reached an asymptote value approximately 7% to 9% higher than the initial condition after approximately 180 minutes of rest.

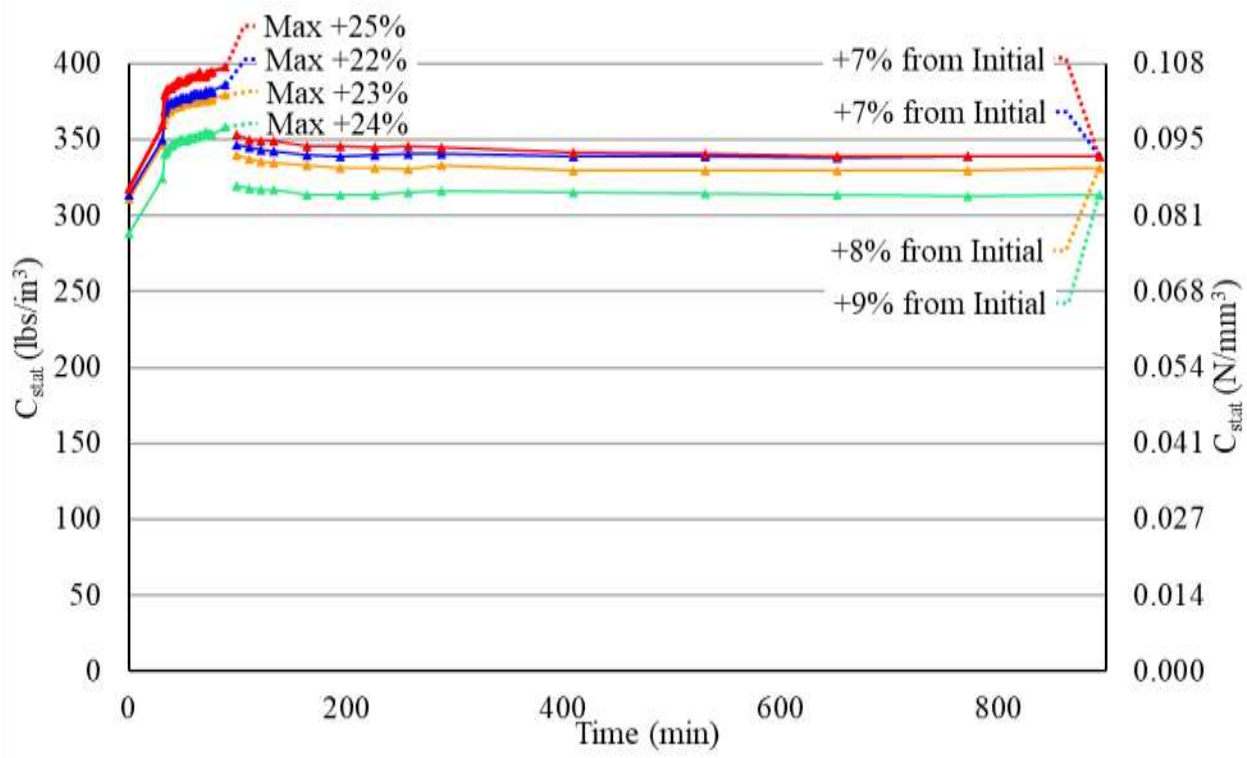


**Figure 3.12 Continuous loading stiffening and preload recovery results**

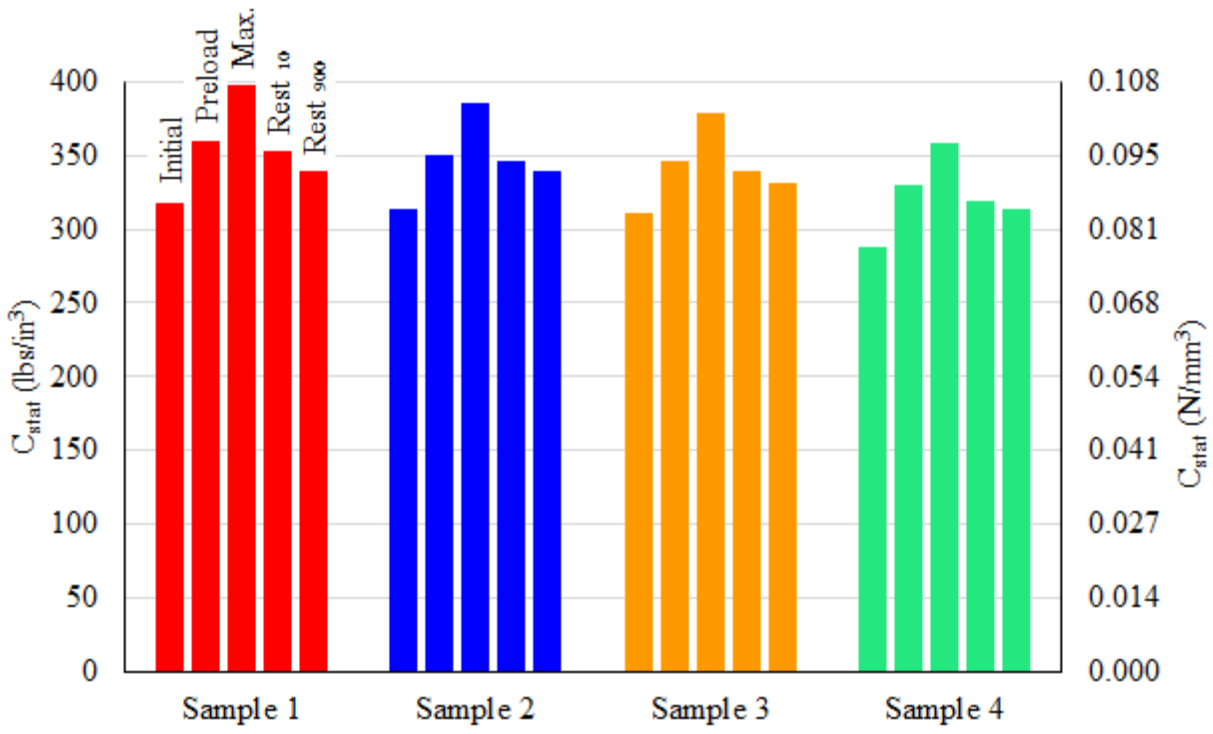


**Figure 3.13 Summary of continuous loading stiffness test results**

Finally, for all samples tested, results shown in Figure 3.14 demonstrate similar trends in behavior; an initial stiffening occurs due to the preload conditioning phase, followed by a gradual stiffening to an asymptotic value of the samples with increased number of simulated train passes. Amplitudes of stiffness variations for each train pass are larger for the thinner sample (Type A) and reduce with the increase in sample thickness. Further, for a significance level of 0.05, stiffness variation amplitudes were found to be different across train headways for all samples other than Type C.

The two results reported for Type A represent the same sample that was put through the procedure a second time after approximately one week of rest. Results undoubtedly demonstrate the elastic recovery capabilities of the sample; once unloaded over time, the sample could fully recover and present behavior like the original untested specimen.

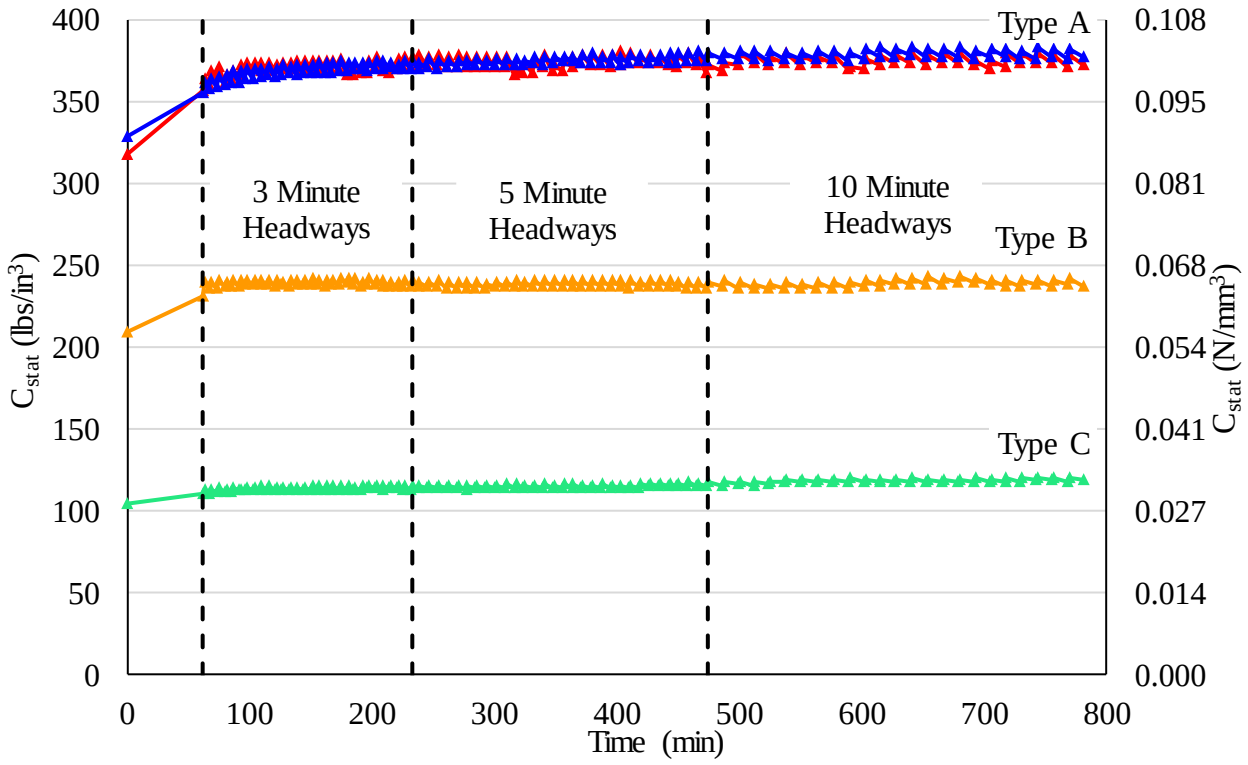


**Figure 3.14 Revenue service traffic loading simulation results**

### 3.3.3 *Insertion Loss Predictions*

Bedding modulus results were also input in the W&K prediction model – detailed in Section 3.2.4 – to determine the resulting insertion loss for each of the different support conditions employed. Values were calculated assuming the UBM was deployed on a ballasted concrete bridge deck for which track and substructure characteristics were chosen based on values obtained from the literature. Insertion loss results were determined for one-third octave band frequencies in the range of interest (i.e. 30 to 200 Hz). Table 3.2 presents the results from all samples and support conditions. Moreover, the bottom section of this table provides a comparison between the resulting insertion losses of concrete and GBP against the control (i.e. steel) as the average insertion loss difference.

For example, considering Type A, the prediction model calculations based on bedding modulus results from a test using concrete as support yielded values of insertion loss 0.6 dB lower on average than the same calculation made based on bedding modulus obtained from the control (i.e. steel support). In contrast, insertion loss based on results from testing using the GBP was 1.7 dB larger on average than the control. This same trend was observed for all sample types.

**Table 3.2 One-third octave band frequency insertion loss results for all samples and support conditions tested**

| One-Third Octave Band Frequency | Insertion Loss Prediction [dB] | | | | | | | | |
|---|---|---|---|---|---|---|---|---|---|
| | Type A | | | Type B | | | Type C | | |
| | Concrete | Steel | GBP | Concrete | Steel | GBP | Concrete | Steel | GBP |
| **31.5** | -1.9 | -2.0 | -1.9 | -1.8 | -1.8 | -0.9 | -0.5 | -0.3 | 0.7 |
| **40** | -1.1 | -0.7 | 0.9 | 1.4 | 1.6 | 3.8 | 4.7 | 4.9 | 6.4 |
| **50** | 3.7 | 4.6 | 7.2 | 7.9 | 8.1 | 10.6 | 11.5 | 11.7 | 13.2 |
| **63** | 13.5 | 14.4 | 17.0 | 17.6 | 17.8 | 20.2 | 21.0 | 21.2 | 22.6 |
| **80** | 20.1 | 21.0 | 23.3 | 23.9 | 24.1 | 26.3 | 27.1 | 27.3 | 28.6 |
| **100** | 14.6 | 15.4 | 17.6 | 18.1 | 18.3 | 20.4 | 21.2 | 21.4 | 22.6 |
| **125** | 12.2 | 13.0 | 15.0 | 15.5 | 15.8 | 17.8 | 18.5 | 18.7 | 19.9 |
| **160** | 10.9 | 11.6 | 13.6 | 14.1 | 14.4 | 16.3 | 17.1 | 17.2 | 18.4 |
| **200** | 10.3 | 11.0 | 13.0 | 13.4 | 13.7 | 15.6 | 16.3 | 16.5 | 17.7 |
| **Average Insertion Loss Difference** | *-0.6* | *1.7* | | *-0.2* | *1.8* | | *-0.2* | *1.2* | |

## 3.4 Conclusions

Laboratory experiments were conducted to investigate the effects of test setup and loading procedure variations on the measurements of under ballast mat (UBM) performance parameters (i.e. static bedding modulus and insertion loss). Three different test support conditions were evaluated together with three different loading pattern simulations conducted to investigate loading effects. Findings from the laboratory experiments are as follows:

- Testing procedures employed proved to exhibit high repeatability for a given sample and support condition, which was within 3.8% of the mean, with the steel providing the least variability among the three supports evaluated.
- Results showed a consistent reduction in bedding modulus for the GBP support, which produced results up to 33.3% lower than the other two support conditions. In contrast, results obtained from concrete and steel supports showed little difference, but concrete tests consistently presented higher values.
- Though consistently lower, GBP results provide evidence to support the proposed adoption of the GBP as a standard equipment for the testing of UBMs. Additionally, applications of this apparatus could extend to the fatigue testing of the material providing a substantially simpler setup when compared to current practices of implementing a ballast box. The study of this proposition will be one of the focuses of Chapter 4.
- Results from simulated loading patterns demonstrated the gradual increase in bedding modulus values with the accumulation of loading cycles over the sample. However, recovery of sample properties was observed to develop at high rates (less than 10 minutes) after load was removed and the UBM could rest.
- Preload results also demonstrated the rapid generation of initial preconditioning stiffening due to a constant static load over the samples at a rate larger than the sensitivity of the test procedure.

- Revenue-service traffic pattern simulations provided evidence of a proposed “working range” stiffness of UBMs. This was in addition to the fact that no effect of traffic density was observed.
- Predictions from a previously-proposed model depicted the influences of the variation of bedding modulus to the studied performance parameters showing differences of up to 1.8 dB, on average, in the insertion loss calculations for the different results from the support condition investigation. This may have a substantial effect on insertion loss performance depending on the level of mitigation needed for a specific application.

# CHAPTER 4: HEAVY HAUL APPLICATION OF UNDER BALLAST MATS – FATIGUE CONSIDERATIONS[3]

## 4.1 Introduction

Application of UBMs in N.A freight lines have grown over the last two decades. Nevertheless, limited research has been conducted to date to evaluate the mechanical fatigue performance of UBMs. Further, the limited number of reports available are based on measurements obtained from samples of a single supplier recovered from field installations (Wettschureck et al., 2002; Dold and Potocan, 2013). Wettschureck (2002) reports on samples recovered after 18 years of service in a 36-kip maximum axle load railway line, resulting in an estimated 45 million load cycles and total 838 million gross tons (MGT). Results reported by Dold and Potocan (2013) refer to samples in service for 21 years under 48.5-kip maximum axle loads for an estimated 17.5 million load cycles.

Furthermore, through conversations with many in the industry, most laboratory studies conducted have been performed for product development purposes and have not been widely made available to the industry. Moreover, the limited literature on this topic is constrained to European applications and testing procedures. Yet, even though installations in countries such as United States, Canada, and Brazil are known of, no reports are available providing insight into the component's performance under heavy axle loads (HAL).

Given the increase in installation frequency and lack of N.A. HAL fatigue performance results, this chapter presents results from laboratory mechanical fatigue tests conducted with two main objectives:

- Compare UBM performance when subjected to European mainline axle loads and N.A. HALs while also exploring the impact on ballast degradation (Section 4.2);

[3] Much of the content from Chapter 4 – Section 4.2 was published in the Proceedings of the 11th International Heavy Haul Association Conference (2017)

- Investigate the feasibility and effectiveness of employing the geometric ballast plate – described in Section 2.1.2 – as an alternative to the ballast box for fatigue performance evaluations (Section 4.3).

## 4.2 Quantifying Effect of N.A. HAL Loads on UBM Fatigue Performance

### *4.2.1 Objective and Scope*

The primary objective of this investigation was to quantify the effects of increased load (i.e. N.A. HAL) on the mechanical fatigue performance of UBMs relative to European testing specifications. During this study, laboratory mechanical fatigue tests were performed on two UBM samples that originated from the same lot. Each sample was subjected to a different load range representing nominal European loads and N.A. HAL, respectively.

A visual assessment of each sample was performed to assess the physical damage incurred as a result of the repeated load cycles. Although potentially not as critical in reducing the ballast stress state in the heavy haul environment, the changes in the UBM bedding modulus were quantified to assess the UBM's ability to retain its noise and vibration mitigation performance. Values were obtained at three different instances: immediately before, within 12 hours after, and 7 days after the repeated loading. Additionally, after the completion of each test (i.e. 2,500,000 cycles), the ballast was collected, and the degradation of the ballast aggregate was quantified by sieve analysis. It is believed that fouling material could further contribute to ballast degradation (Selig et al., 1988; Selig and Waters, 1994; Qian et al., 2014).

### *4.2.2 Materials*

#### 4.2.2.1 Under ballast mat

UBM samples intended for freight traffic loading conditions, labeled "Type A", were used in this investigation (Figure 4.1). The samples are comprised of a profiled mat bonded to a flat protective rubber

layer with a synthetic fiber grid between. Table 4.1 provides details of the sample geometry, including its dimensions and thickness.

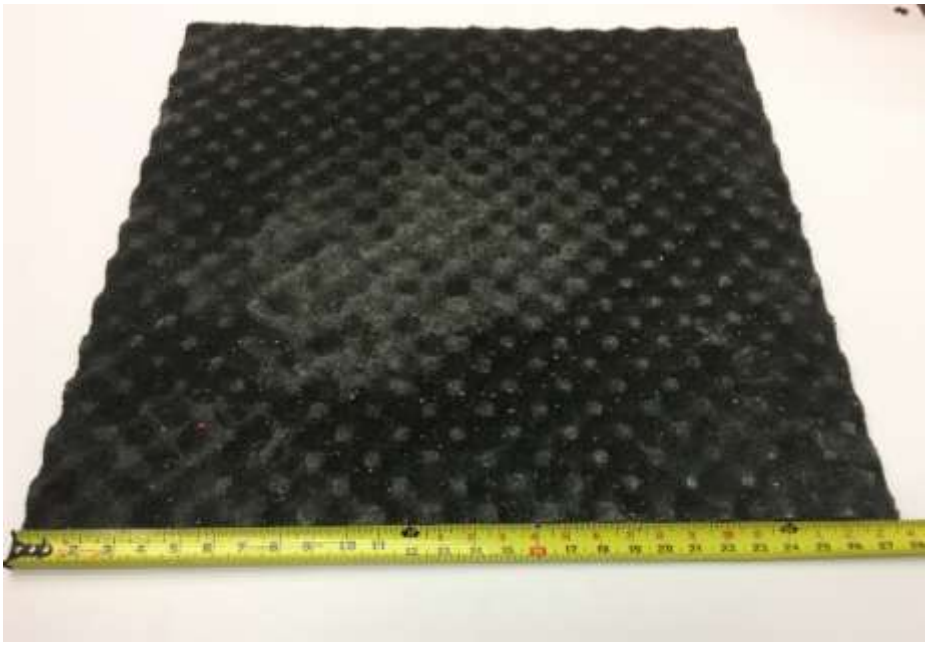

**Figure 4.1 Under ballast mat sample employed in a ballast box fatigue tests**

**Table 4.1 Under ballast mat sample characteristics**

| Label | Mat Thickness [in. (mm)] | | Sample Size [in. (mm)] | Construction |
|---|---|---|---|---|
| | Minimum | Maximum | | |
| Type A | 0.197 (5) | 0.394 (10) | 27.5 (699) x 27.5 (699) | Profiled mat bonded to flat protective layer |

#### 4.2.2.2 Ballast

Ballast material used for this investigation originated from a quarry commonly used by a N.A. Class I railroad and was stored in a stockpile at the laboratory facility. The coarse aggregate material consisted of crushed granite with uniformly graded particle size distribution compliant with the American Railway Engineering and Maintenance-of-way Association (AREMA) No. 4A gradation recommendations (AREMA, 2012). Figure 4.2 shows the original gradation for the ballast material employed along with

the AREMA specified gradation limits for No. 4A ballast. To ensure the quality and uniformity of the ballast used for each test, all ballast was washed, oven dried, and sieved to remove all fines from its initial state. For this research study, fines were considered as all particles passing the ⅜-inch sieve or smaller than 9.5 mm (Qian et al., 2014). Ballast material was recombined and mixed using the recommended practices from AASHTO T 248, mixing and quartering procedures from Method B were employed due to the large size of the sample (AASHTO, 2011).

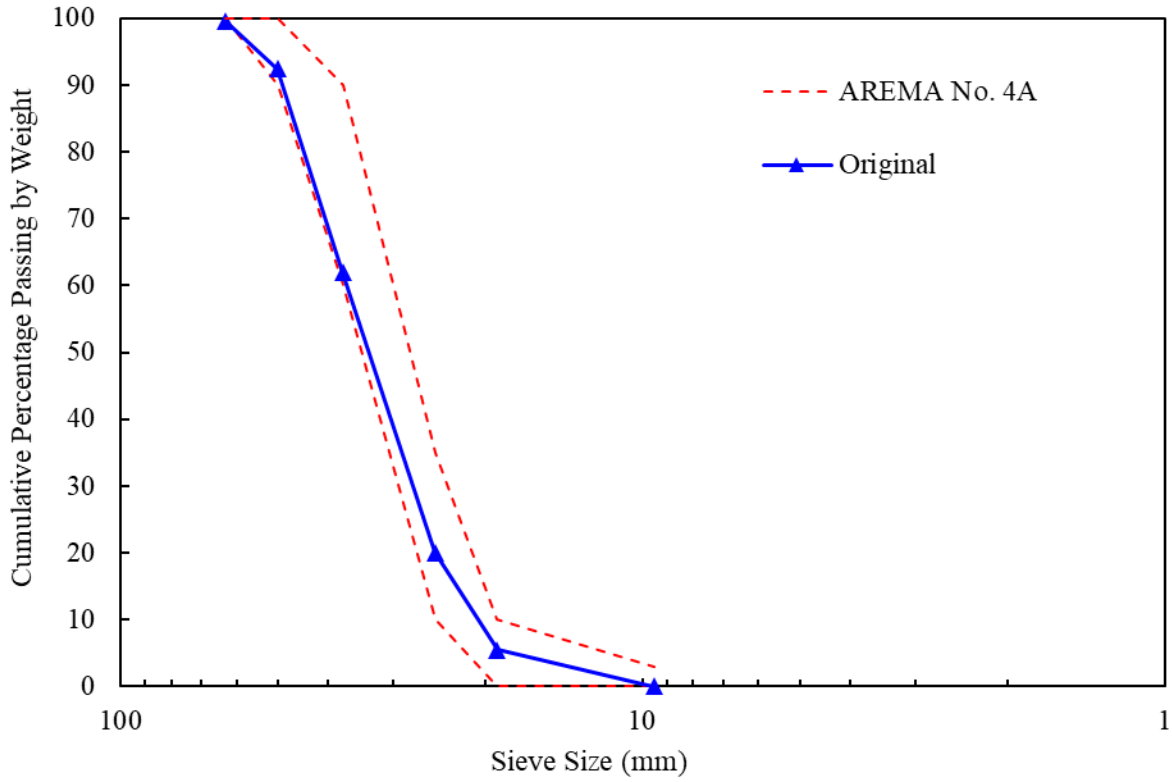


**Figure 4.2 Original particle size distribution of granite material**

### *4.2.3 Laboratory Experimentation*

Laboratory tests performed as part of this study followed modified recommendations from the German Deutsches Institut für Normung (DIN) 45673-5 standard (hereinafter referred to as DIN) for the determination of the mechanical fatigue resistance of under ballast mat samples (DIN 2010).

#### 4.2.3.1 Test setup

The construction of the test setup utilized the newly designed UIUC ballast box and loading plate (described in Section 2.1.2) due to space constraints in the testing frame. The UBM sample was placed on the bottom of the box over the flat steel bottom. To better simulate particle confinement experienced in the field, one-quarter inch (6.35 mm) thick neoprene sheets were placed along the sidewalls. Clean ballast – obtained from the processes described in Section 4.2.2.2 – was added and compacted for 90 seconds in three 4-in. (10.2-cm) lifts; an adjustable formwork vibrator attached to a steel plate provided a 1000-lbf (4.4-kN) compaction force at 60 Hz. Figures 4.3 and 4.4 show the compaction process and the finished setup respectively.

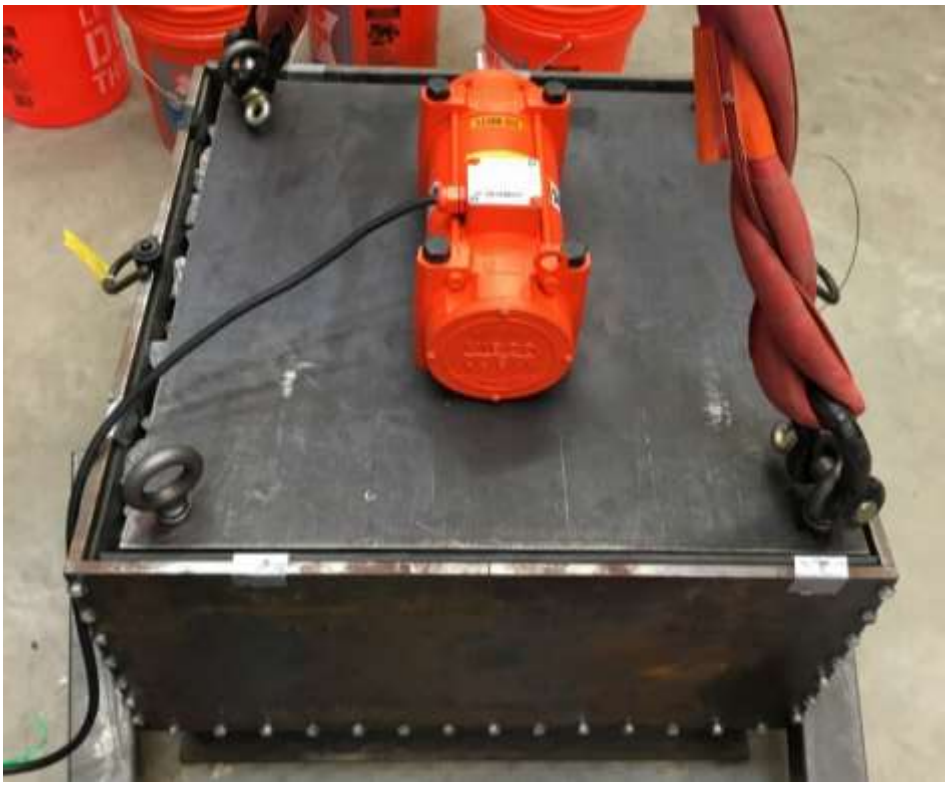

**Figure 4.3 Compaction of ballast layer using vibratory plate**

**Figure 4.4 Finished compacted ballast layer in the UIUC ballast box**

### *4.2.4 Test Procedures*

Modified mechanical fatigue testing procedures, detailed in Section 2.2.2, were used during this investigation. Results are presented for tests using only the second stage of the DIN recommended procedures. This was deemed sufficient to generate results for a performance comparison between the two loading conditions and additional details are discussed in Chapter 2.

Qualitative and quantitative assessments of the UBM performance and ballast particles were performed during the tests as follows:

- Physical assessment of damages incurred to the specimens
- Static bedding moduli ($C_{stat}$) for each evaluation range – as described in Section 2.2.1 – prior-to and subsequent-to the applied fatigue loading
- Ballast material particle size distribution as per ASTM C136

Loads were determined as described in Section 2.2.2.1 and are summarized in Table 4.2.

**Table 4.2 Loading procedures employed during comparison fatigue tests**

| Loading Scenario | Loading Range [kips (kN)] | | Sinusoidal Frequency [Hz] | No. of Cycles |
|---|---|---|---|---|
| | Minimum | Maximum | | |
| European | 0.4 (1.8) | 5.8 (25.8) | 5 | $2.5x10^6$ |
| North American | 0.4 (1.8) | 9.4 (41.6) | 5 | $2.5x10^6$ |

### *4.2.5 Results*

After each test the ballast box was deconstructed and ballast material was collected, and the UBM samples were thoroughly evaluated for physical damage. The sample tested to European loads displayed minor surface wear and compression spots immediately after testing. However, all areas initially displaying wear and compression were able to recover after just a few days of rest (i.e. no loading). Likewise, little signs of physical damage could be assessed on the sample tested to N.A. loads. In like manner to the European sample, most compression marks observed in the N.A. sample were able to recover. However, even after a few days of rest, there were still clear ballast particle imprints and minor superficial tears present around some of the existing compression marks accompanied by signs of wear due to particle attrition against the UBM surface (Figure 4.5). Yet, ballast particles did not puncture through the protective layer, being smaller than 0.5 in. (12.7 mm) long, 0.1 in. (2.5 mm) wide and 0.08 in. (2 mm) deep. No damage incurred to either sample was considered to be detrimental to the performance of the component.


**Figure 4.5 Superficial damage incurred to N.A. sample (ruler scale in inches)**

As mentioned previously, bedding modulus values were calculated for both evaluation ranges of each UBM prior-to and after fatigue testing. All obtained results are presented in Table 4.3. Though all samples were evaluated for both ranges, the percent change in bedding modulus is most relevant within the range compatible to the fatigue loading scenario of each sample (e.g. European evaluation range is most applicable to the European loading scenario, etc.).

**Table 4.3 Bedding modulus results after ballast box fatigue tests**

| Loading Scenario | Stage | Evaluation Range | | | | | |
|---|---|---|---|---|---|---|---|
| | | European | | | North American | | |
| | | $C_{stat}$ | | %Δ | $C_{stat}$ | | %Δ |
| European | Initial | **309** | (0.084) | | 360 | (0.098) | |
| | After | **340** | (0.092) | **10%** | 395 | (0.107) | 10% |
| | 1-week | **301** | (0.082) | **-3%** | 359 | (0.097) | 0% |
| North American | Initial | 316 | (0.086) | | **370** | (0.1) | |
| | After | 540 | (0.147) | 71% | **617** | (0.167) | **67%** |
| | 1-week | 342 | (0.093) | 8% | **398** | (0.108) | **8%** |

*Note: Units in $lbs/in^3$ ($N/mm^3$)*

From the presented results, there is a clear difference in the bedding modulus performance metric immediately after the completion of the fatigue loading. This can be observed across the two tests with variation in bedding modulus being higher for the N.A loading scenario than the DIN recommended European loading condition. It is hypothesized that larger amounts of elastic deformation with lower rate of recovery develop due to the higher loads, which in turn stiffens the component as attested by an increase in bedding modulus results immediately after the test.

However, results obtained after a one-week rest period depict bedding modulus values much smaller than those obtained immediately after the completion of the fatigue loading – 8% and -3% for N.A and European samples respectively – indicating elastic recovery. This value is important considering a rest period naturally exists in revenue service with train headways and should to be taken into consideration in situations where UBM are sought to achieve a desired vibration attenuation in heavy haul railway lines. The observed negative percentage change in final static bedding modulus value for the European sample may point to the accuracy of the testing procedures in place (i.e. margin of error).

To provide researchers with additional insight into the effects of the higher loads on track deterioration, ballast gradation results were obtained in both tests. These results are presented in Figure 4.6 indicating no significant damage to the ballast particles from repeated loading. A qualitative visual assessment conducted during the collection of the particles showed little-to-no signs of particle

breakage. However, the presence of fines within the ballast material was noted after both load levels. This assessment, together with small shifts in the gradation curve, are thought to be related to particle surface wear of the aggregates caused by the relative movement between particles during loading and unloading cycles.

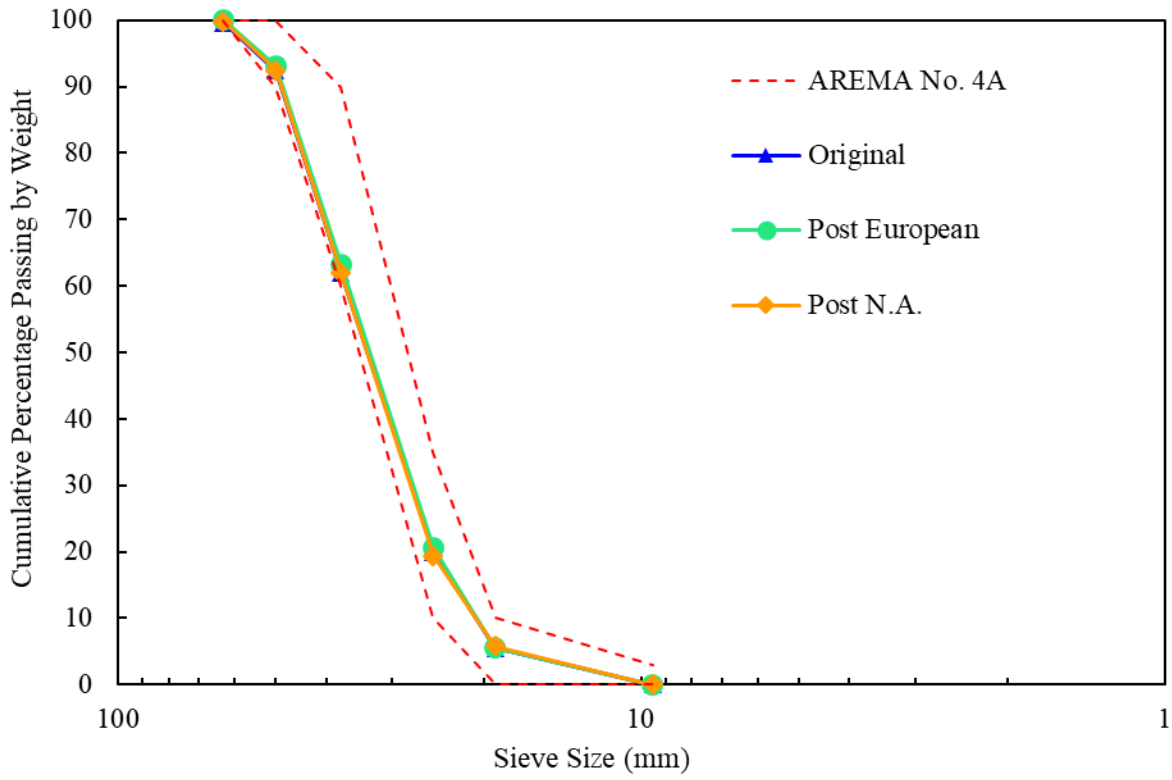


**Figure 4.6 Particle size distribution of the granite ballast material before and after testing**

As previously mentioned, material passing the ⅜-inch (9.5-mm) sieve was defined as fines within this study and discarded prior to construction of the box. Accordingly, an estimate of fine material produced can be drawn from the difference in weight between the initial and final conditions of the material. Such conclusion can only be drawn based on the assumption that loss of material was due to the generation of particles finer than the employed sieve threshold. Unfortunately, due to issues during the

laboratory procedures, an exact loss amount cannot be provided for each individual case. Yet, for both tests the loss in weight of the original material employed was below 1.5%.

### *4.2.6 Ballast Box Fatigue Summary*

Tests were conducted to assess the mechanical fatigue resistance of two UBM samples under different simulated loading conditions, N.A. HAL and European mainline. A qualitative assessment of the physical samples was performed prior-to and following tests conducted. Although there were slightly more areas of damage as a result of the N.A loading, both samples displayed negligible physical damage as a result of the load through a qualitative visual assessment. Given the samples showed no significant damage, this particular UBM could withstand both N.A and European loading environments. Further, the results indicate that an increased load level evaluation seems reasonable to be employed for UBMs intended for heavy haul lines.

The UBM subjected to N.A. HAL displayed a larger reduction in vibration mitigation performance when quantified immediately after the completion of the fatigue testing than the UBM subjected to European loading (67% change vs 10%, respectively). However, this difference became negligible for the test case after approximately one week. Undoubtedly, these results are important when considering that a rest period naturally exists between revenue service load applications and can allow the recuperation of the component. Further, given vibration attenuation is not typically the primary function of UBMs on heavy haul lines, this UBM should be able to serve the primary purpose of reducing the stress state on ballasted bridge decks or in tunnels. That said, if vibration attenuation is a key objective of the installation, then an increased load level evaluation can provide a better approximation of the component performance in revenue service. Finally, the gradation analysis results demonstrated that no significant ballast breakage occurred during either test, further supporting the effectiveness of the UBM in these loading environments.

This testing has provided researchers and practitioners with information about the importance of case-specific testing procedures for proper assessment of the fatigue performance of UBMs.

Additionally, the compelling effects of sample rest period to the determination of changes in the bedding modulus parameter were also demonstrated and should be carefully considered when developing recommended practices.

## 4.3 Fatigue Testing with the Geometric Ballast Plate

### *4.3.1 Objective and Scope*

Selig (1994) describes traditional characteristics of ballast as "[…] angular, crushed hard stones and rocks, uniformly graded, […]". However, there exists no thorough agreement on the specific characteristics to which ballast should conform. Various organizations (International Union of Railways (UIC) and AREMA, etc.) provide desirable ballast material characteristics within their published documents, most focused on particle sizes leading to a wide range of possible combinations of ballast material characteristics. Material variations become even more pronounced as parameters given in the AREMA Manual of Railway Engineering (AREMA, 2012) require only particle elongation features be measured – to mitigate particle breakage under load – but do not specify ballast particle angularity features. Stemming from these considerations, large intrinsic variability is present in any testing procedure employing real ballast materials as a contact interface. Assessments of fatigue performance, as the one conducted in Section 4.2 above, are one of such tests influenced by changes in particles shape characteristics. To avoid these influences, the standardized geometric ballast plate (GBP) was adopted for the development of fatigue tests in this section given it is a standardized tool developed by European researchers as described in Section 2.1.2.

In conjunction with the rationale presented, the use of the GBP also provides a greater ability for monitoring gradual changes in UBM performance allowing for partial measurements of material characteristics without the need of a complete deconstruction of the test setup – as is the case for all ballast box tests. This will be discussed in more detail in Chapter 6 as part of the future work for this study.

Laboratory experiments were developed to investigate the effectiveness of using the GBP as a substitute to the ballast box during fatigue performance evaluations. Furthermore, the recently published EN 16730:2016 (BS EN 16730, 2016) for testing of USPs already recommends similar tests with the GBP setup in the evaluation of the fatigue performance of USPs intended for vibration attenuation.

### *4.3.2 Laboratory Experimentation*

#### 4.3.2.1 Material

The UBM material employed in these experiments was selected to maintain consistency with the previously conducted ballast box fatigue tests – Section 4.2 – and allow researchers the ability to compare and contrast results between the two test methods (i.e. ballast box vs GBP). Samples were cut, from the same roll of Type A UBM, in 10 in. by 10 in. (25.4 cm by 25.4 cm) squares (Figure 4.7). These dimensions are also the same used in all experiments presented in Chapter 3 for consistency.

**Figure 4.7 Type A UBM cut sample for GBP fatigue tests**

#### 4.3.2.2 Test Setup

Tests were conducted using a similar setup to the one employed in the evaluation of support condition effects presented in Section 3.2.2.1. The GBP was placed over the support concrete block inside the Pulsating Load Testing Machine's (PLTM) frame and fixed to the frame's floor by braces to ensure no movement of the plate during the repeated load tests (Figure 4.8). Thermocouples, attached to each sample at both the center and edge locations, were deployed to monitor temperature changes in the UBM sample during tests and assure no heat build-up occurred (Figure 4.9). Additionally, ambient temperatures were monitored to provide added context to sample temperature variations.

**Figure 4.8 GBP fatigue test setup**

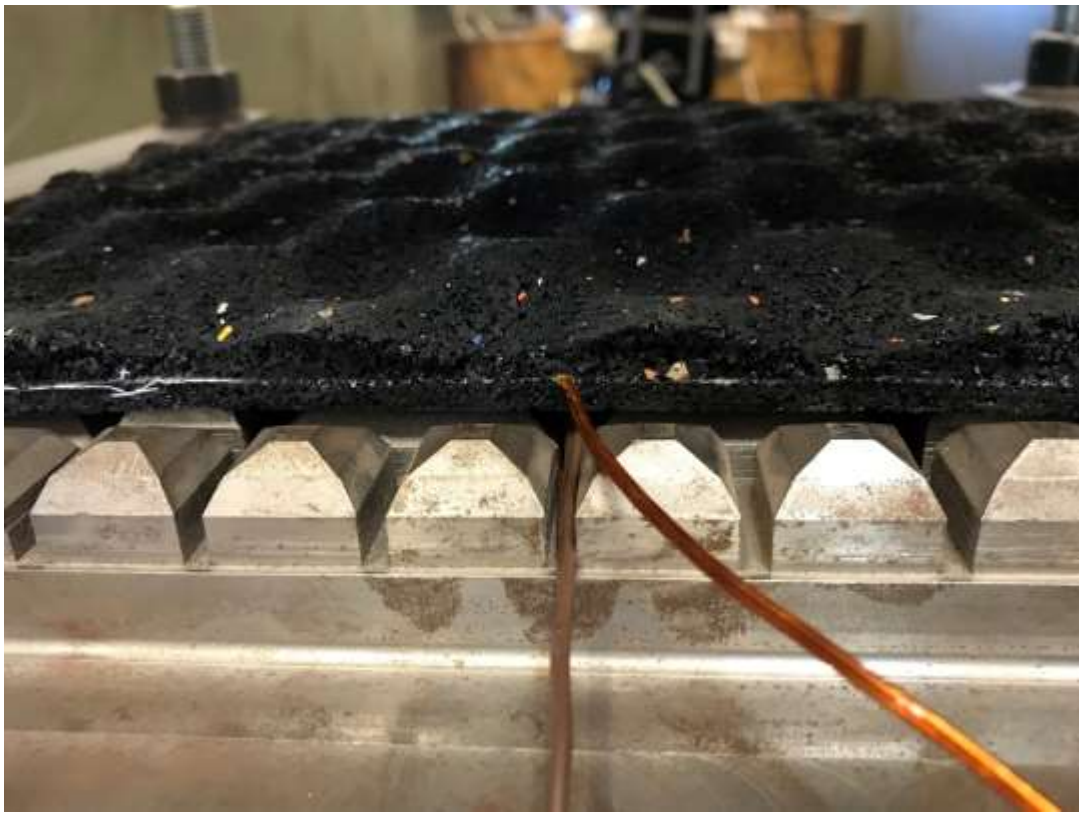

**Figure 4.9 Thermocouple placement on UBM sample during testing**

#### 4.3.2.3 Test Procedures

Procedures maintained consistent load application frequencies and number of cycles as tests ran with the ballast box and described in Section 2.2.2. New load magnitudes were determined based on the estimated pressures acting on the UBM samples during ballast box test cases representing European and N.A. HAL (Section 4.2). Talbot's pressure distribution equation (Equation 4.1) (Talbot, 1920) was used to estimate these pressures based on the corresponding applied loads in Section 4.2. Maximum stresses – and corresponding loads – to be applied to the UBM samples during GBP fatigue tests were determined as described and are presented in Table 4.4.

$$p_c = \frac{16.8 p_a}{h^{1.25}} \quad (4.1)$$

where, $p_c$ = pressure at given point at depth "$h$"

$p_a$ = average pressure on bottom of tie (assumed equal to pressure at ballast box loading plate)

$h$ = depth of ballast

**Table 4.4 GBP fatigue loading conditions**

| Loading Scenario | Loading Range [kips (kN)] | | Sinusoidal Frequency [Hz] | No. of Cycles |
|---|---|---|---|---|
| | Minimum | Maximum | | |
| European | 0.4 (1.8) | 3.9 (17.2) | 5 | $2.5 \times 10^6$ |
| North American | 0.4 (1.8) | 6.3 (27.8) | 5 | $2.5 \times 10^6$ |

### *4.3.3 GBP Fatigue Results and Discussion*

Static bedding modulus values obtained before and after each test, in accordance with the procedures presented in Section 2.2.1, are presented in Table 4.5. Note that static bedding modulus values are calculated for each respective evaluation range as per Table 2.1.

**Table 4.5 GBP fatigue bedding modulus results**

| Test Type | Sample | $C_{stat,Initial}$ | | $C_{stat,After}$ | | %Δ |
|---|---|---|---|---|---|---|
| European | #1 | 262.4 | (0.071) | 290.3 | (0.079) | *11%* |
| | #2 | 321.7 | (0.087) | 336.8 | (0.091) | *5%* |
| North American | #3 | 343.6 | (0.093) | 372.9 | (0.101) | *9%* |
| | #4 | 337.0 | (0.091) | 366.4 | (0.099) | *9%* |

*Note: Units in $lbs/in^3$ ($N/mm^3$)*

In the above results, samples #3 and #4 (tested under N.A HAL) display identical percent changes in performance after the end of the tests. Meanwhile, a larger spread in results is seen for samples tested

under European loads with percent change results larger than the N.A tests. Overall, all samples displayed small changes in static bedding modulus (Table 4.5) when compared to values obtained from the DIN recommended ballast box test procedures (Table 4.3). Results obtained are comparable to ballast box 1-week static bedding modulus values which further provides evidence that ballast box tests might represent harsher conditions to the samples compared to the GBP fatigue setup.

Similar to results obtained in Section 4.2, a visual assessment found imprints from the GBP contact points on the UBM samples after testing. Recovery of these deformations was also observed to be similar to cases in Section 4.2 with imprints fully recovering for the European samples but only partially for the N.A. samples. Moreover, samples subjected to N.A. loading conditions showed the formation of shallow cracks of the protective layer around the edges of the contact points between sample and GBP, as can be seen in Figure 4.10. Again, these effects could not be observed in samples tested under European loading conditions. This may be correlated to the same damages caused by the contact between the UBM and the edge of ballast particles (Figure 4.5). It is believed that the developed cracks are formed by tearing of the specimen as the sample is compressed and material in contact with the profile of the GBP is held by frictional forces while free material tries to deform into the grooves of the GBP.

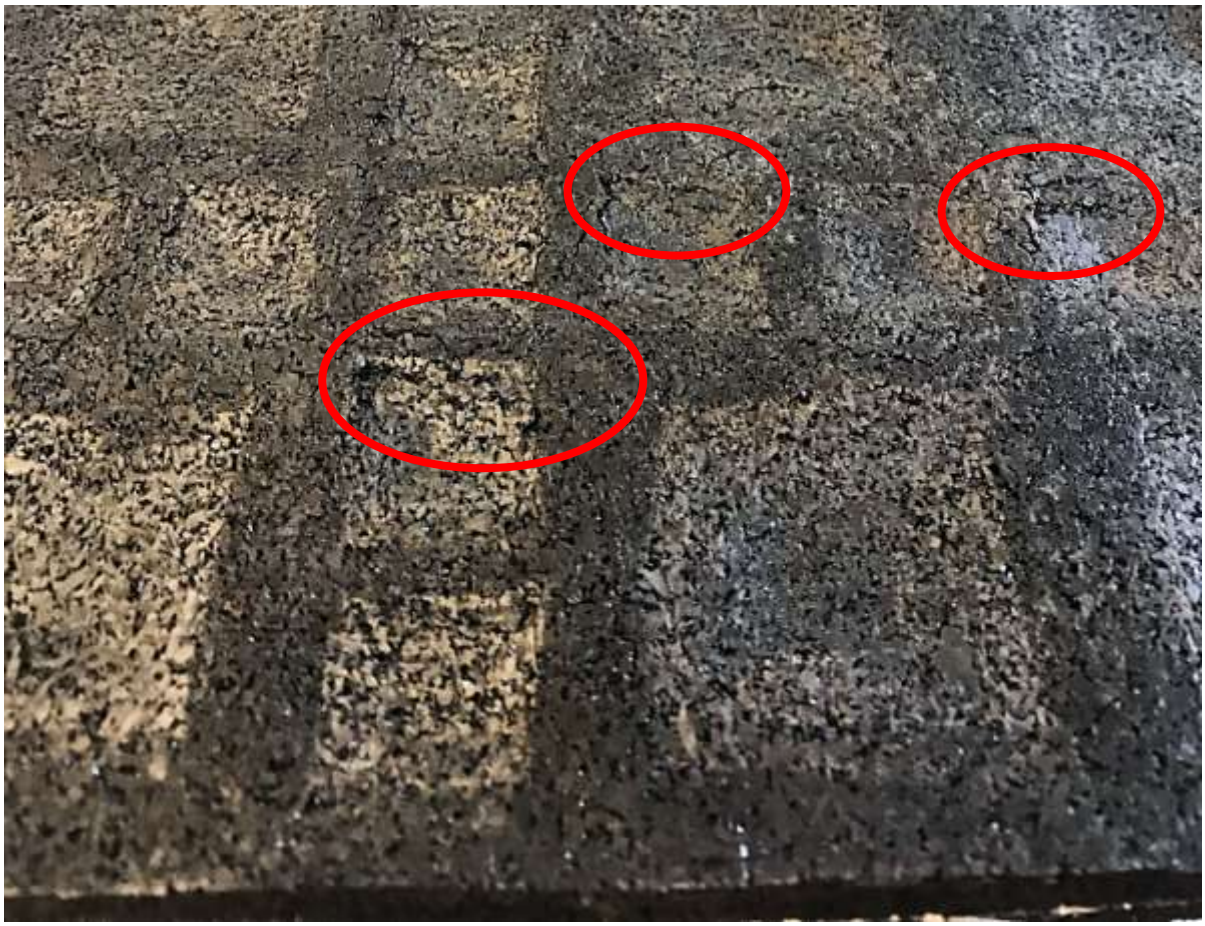

**Figure 4.10 Example of cracks developed at edges of contact points for sample #3**

Thermal aging – due to exposure to increased temperatures – can also result in degrading conditions for elastomer materials (Mars and Fatemi, 2004), so temperature monitoring was of importance to ensure no heat build-up occurred during tests. Time-history plots of temperature variation for each test conducted are presented in Figure 4.11. Temperature monitoring of all samples during testing showed normal daily fluctuations of sample temperature parallel to variations in ambient temperature readings. Maximum temperature values recorded during testing were of 92.5°F (33.6°C) – sample #3 – which were below the DIN specified limit of 104°F (40°C). Note that instrumentation failure during testing with sample #3 restricted the collected data to a single sample sensor (center) and only a portion of the test duration. Nevertheless, a similar behavior to all other samples can be observed.

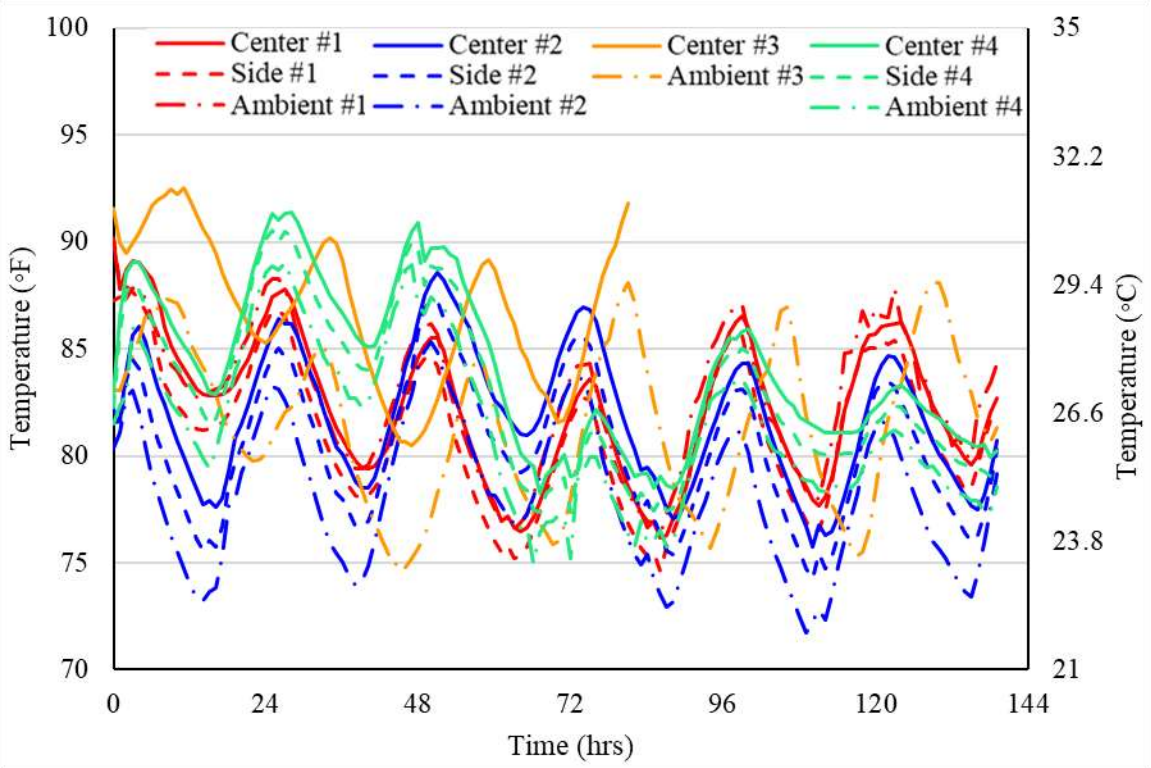


**Figure 4.11 Temperature variation time-history plot for all tests**

## 4.4 Conclusions

As part of this study, UBM samples were subjected to repeated fatigue loading in a ballast box simulating a section of track and over a standardized geometric ballast plate (GBP). Two loading scenarios were used to represent N.A heavy axle loads (HAL) and European mainline axle loads. The main objectives were to: (i) quantify the effect of increased loads and (ii) quantify effects of different test setups on the UBM physical health assessment and the change in bedding modulus of the samples. Additionally, degradation trends of the ballast material used during ballast box testing were monitored.

Comparison of effects obtained from both test setups demonstrated similar results in terms of physical damage incurred. Samples tested under N.A. loading conditions displayed superficial tears around edges of contact points – either ballast particle or profile edge – but none capable of penetrating further than the superficial protective layer of the UBM. Tears caused by ballast particles did appear to

be accompanied by minor wear, most likely due to rubbing actions from the moving particle with loading. In a similar manner, sample deformation at the contact points were noticeable on all samples after testing, but only N.A. samples partially retained these after resting unloaded for approximately seven days. Meanwhile, samples tested under European loading conditions showed marginal signs of physical damages independent of the test setup employed.

Overall, the minimal amount of physical damage observed on all samples tested is not believed to negatively influence the performance of the component in revenue service especially since the simulated loading conditions represent much harsher circumstances than in-service conditions UBMs are subjected to. These results demonstrate the GBP to be an effective alternative to the ballast box in assessing the physical fatigue behavior of UBM samples at different load levels while also providing considerable simplification of test execution.

Static bedding modulus assessments showed more intriguing results in terms of comparison between the two employed test setups. The GBP test samples presented bedding modulus changes much smaller than the corresponding samples tested using the ballast box setup for the conditions directly after the end loading cycles. Results are more comparable to ballast box results after rest, indicating that the GBP setup may provide a lesser degrading environment for the sample. However, it is believed that the after-rest condition is a more realistic approximation of the revenue service conditions to which samples are subject to, due to component rest during train intervals. Further, based on the experience obtained throughout this study, the variations in percent changes between N.A. and European results – 8% vs. -3% and 9% vs. 5%/11%) – may be most associated with test and sample variability than differences in the effects of each simulated scenario. This understanding further supports the effectiveness of the GBP setup to serve as an alternative method for quantifying the fatigue performance of UBM components.

Lastly, the monitored conditions of the ballast material throughout the ballast box tests demonstrated the setup – and/or procedure – to be unable to generate enough degradation of the ballast material to provide insight as to the ballast degradation behavior under such loading conditions. As will be demonstrated in Chapter 5, additional tests developed as part of this research showed that under rigid

conditions (i.e. no UBM installed) the ballast box test is unable to simulate degradation conditions seen in revenue service.

All the same, it is important to consider that any attempted comparison between the effectiveness of each one of the employed test setups must consider the differences in test constructability, with the GBP setup providing an extreme ease of assembly and condition monitoring during testing while also providing comparable results to the ballast box test. In addition, the use of the simplified GBP setup may provide additional benefits in allowing for assessments of partial development of sample degradation based on bedding modulus – or other metric – obtained at smaller intervals during tests without the need for disturbing the setup.

# CHAPTER 5: IMPACTS OF UNDER BALLAST MATS ON THE IMPROVEMENT OF DIFFERENTIAL MOVEMENTS IN TRACK TRANSITION ZONES[4]

## 5.1 Introduction and Background

Railway transition zones characterize areas in the rail network where an abrupt change in track stiffness occurs; these include tunnels, at-grade crossings, special trackwork, and bridge and culvert approaches. Trains interacting with these track sections experience sudden variations in vehicle/track interaction forces (Dahlberg, 2003). Railroad personnel have long reported these zones as problematic, engendering rapid development of track geometry issues and endangering a railroads efficiency due to increased maintenance requirements, delays, or slow orders (Hunt, 1997; Frohling et al., 2005; Sasaoka and Davis, 2005; Briaud et al., 2006; Jenks, 2006; Lundqvist et al., 2006; Woodward et al., 2007; Banimahd et al., 2012). Moreover, maintenance and renewal expenses related to transition zones comprise a sizable share of a railroad's annual operating expenses with reported annual expenditures ranging from 110 to 200 million US dollars for European and N.A railroads respectively (ERRI, 1999; Hyslip et al., 2009; Sasaoka and Davis, 2005).

Substantial research has been conducted to investigate railway transition zone problems and the mechanisms that drive its accelerated deterioration (Nicks, 2009; Li and Davis, 2005; Coelho et al., 2010; Varandas et al., 2011; Tutumluer et al., 2012; Mishra et al., 2012; Wang et al., 2015; Stark and Wilk, 2016). Li and Davis (2005) attributed problems to three proposed major causes: (i) change in track stiffness leading to uneven track deflections under moving loads; (ii) differential settlement between approach and bridge sections; and (iii) geotechnical issues due to material quality, insufficient consolidation, and compaction of the substructure and/or inadequate drainage. Sasaoka and Davis (2005) listed differential settlement, stiffness characteristic differences, and track damping properties as the most important parameters influencing transition zones problems. Although different authors attribute root

[4] Much of the content from Chapter 5 was published in the Proceedings of the 10th International Conference of the Bearing Capacity of Roads, Railways and Airfields (2017)

causes of the problems in transition zones to different individual issues, an agreement exists as to the importance of track stiffness properties.

According to Li & Davis (2005), differential vertical movements of the track profile vary significantly between the approach and the structure. Due to differences in substructure conditions, the approach section undergoes higher deformations than the structure under loading conditions, resulting in the phenomenon referred to as differential movement. Reported driving mechanisms of differential movements include the abrupt changes in track stiffness and damping properties of the track structure and/or foundation, and settlements due to ballast degradation and/or subgrade and fill layers (Li and Davis, 2005; Selig and Waters, 1994; Mishra et al., 2012; Sasaoka and Davis, 2005; Nicks, 2009; Tutumluer et al., 2012).

It is important to understand that the issues at transition zones are not singular to one phenomenon or component, but constitute a system problem that requires a holistic investigation. Accordingly, differential movements instigate a negative feedback loop followed by plastic deformations of the approach, increased impact loads, ballast deterioration, and additional track settlements spawning accelerated deterioration loops of the track, and of other components and/or structures.

Railway transitions are regularly subjected to high impact loads from heavy axle loads traversing sections of differential stiffness, thus leading to accelerated substructure degradation. Ballast is a vital component of this substructure and therefore to the bearing capacity of railway tracks. There are two primary mechanisms by which ballast particles degrade. First, attrition, defined as the deterioration of the surface texture and geometry of the ballast particles removing surface texture and angular characteristics of aggregates that are critical to the sustainability of the structural skeleton providing ballast with its load bearing capabilities and resistance to permanent deformation (Tutumluer and Pan, 2008; Lu and McDowell, 2010; Wnek et al., 2013). Second, breakage, defined as the tensile failure of the ballast particles due to exceedingly high contact stresses between individual stones, resulting in material splitting (Selig and Waters, 1994; Wang et al., 2017). Both above-mentioned mechanisms contribute to ballast fouling (Selig et al., 1988; Selig and Waters, 1994; Qian et al., 2014).

For decades, railroads and researchers have explored the use of elastic resilient materials in the track structure. Three primary components have been used to provide solutions by railroads to manage the elastic properties of railway track, these are: premium elastic fastening systems, under sleeper pads (USP), and under ballast mats (UBM).

In recent years, a consistent increase in the use of UBMs in freight railroad environments has provided opportunities to explore and report their potential effectiveness for mitigating transition zone problem and/or reducing ballast stresses (Indraratna, 2016; Sol-Sánchez et al., 2014; Li and Maal, 2015; Indraratna et al., 2014; Sol-Sánchez et al., 2015).

The UBM is a resilient pad that can provide additional resiliency to the track structure foundation and effectively dissipate energy – manifested in the form of vibrations that propagate through the ballast structure – from the wheel-rail and/or tie-ballast interfaces that are associated with accelerated rates of ballast degradation (Sol-Sánchez et al., 2014). Kerr & Moroney (1993) traced the transition zone problem to the sudden changes in accelerations of the wheels and vehicles at these interfaces and cited key remediation methods aimed at reducing these changes, such as the reduction of vertical stiffness on the "hard" side of the transition. Despite the potential for UBMs to address the abrupt changes in track stiffness and mitigate differential movements at problematic track transition zones, there is little to no documentation available in the literature.

## 5.2 Objective and Scope

The primary objective of this chapter is to investigate the effect of UBMs on the transient deformation behavior of track sections built over stiff substructures such as bridge decks, and subjected to cyclic loading. In this chapter, ballast vertical deformation measurements under cyclic load are presented. Measurements were obtained during laboratory fatigue experiments conducted on an UBM sample. Ballast degradation trends were quantified through laboratory sieve analyses with ballast gradations compared prior to and after testing. This chapter presents results of the laboratory tests conducted and

compares them with field measurements of transient deformations obtained in bridge approach sites in N.A. from previous literature.

## 5.3 Materials

### 5.3.1 *Under Ballast Mats*

"Type A" UBM samples, designed for freight traffic loading conditions, were used during the experiments presented in this chapter (Figure 5.1). Table 5.1 provides details of the sample geometry including its dimensions and thickness.

**Figure 5.1 Type A UBM sample designed for freight loading**

**Table 5.1 Under ballast mat sample characteristics**

| Label | Mat Thickness [in. (mm)] | | Sample Size [in. (mm)] | Construction |
|---|---|---|---|---|
| | Minimum | Maximum | | |
| Type A | 0.197 (5) | 0.394 (10) | 27.5 (699) x 27.5 (699) | Profiled mat bonded to flat protective layer |

### 5.3.2 *Ballast*

Granite ballast material used for this investigation originated from the same quarry commonly used by a N.A Class I railroad as described in Chapter 4 having a uniformly graded particle size distribution compliant with the AREMA No. 4A gradation recommendations (AREMA, 2012). Figure 5.2 illustrates the original particle size distribution – showing minimal differences from the material employed in Chapter 4 (Figure 4.3) – for the ballast material employed along with the corresponding AREMA gradation limits. All ballast material was washed, oven dried and sieved to ensure no fines were present in the initial state of the sample. As was discussed in Chapter 4, fines were considered as all particles smaller than 9.5 mm or passing the ⅜-in. sieve (Qian et al., 2014). Separated ballast material was then recombined and mixed using the recommended practices from AASHTO T 248 - Method B due to the large size of the sample (AASHTO, 2011).

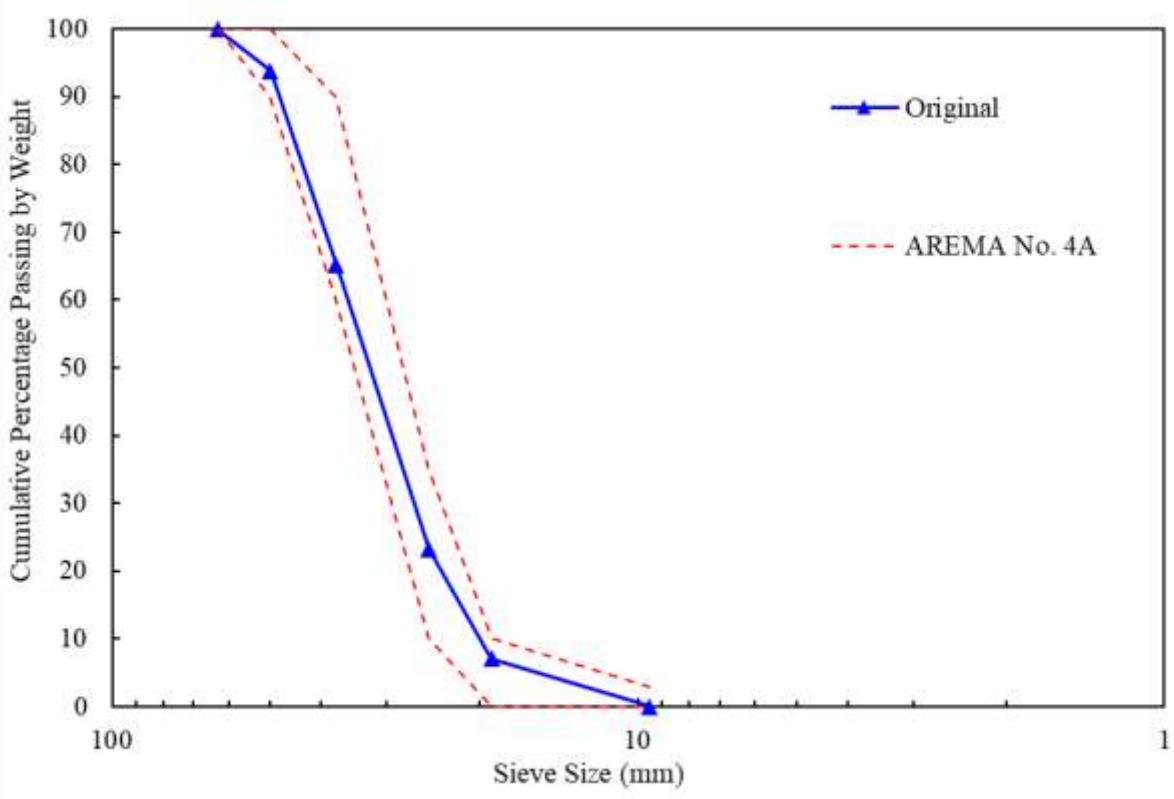


**Figure 5.2 Particle size distribution of granite ballast material**

## 5.4 Laboratory Experimentation

Laboratory tests performed as part of this study followed recommendations from the German DIN for the determination of the mechanical fatigue resistance of under ballast mat samples.

### 5.4.1 *Test Setup*

Due to space constraints of the test frame available for testing, ballast box and loading plate had to be redesigned as described in Section 2.1.2. Figure 5.3 shows the UIUC ballast box and loading plate setup.

**Figure 5.3 Constructed UIUC ballast box and loading plate setup with additional instrumentation**

The applied loads and stresses at the plate/ballast interface in the setup were specified according to the DIN standard. To maintain the same stress levels of the DIN standard, the applied loads during testing were scaled based on the new loading plate area used in this study. Details of the applied load levels are presented in the subsequent section.

Two complete setups for testing were constructed using the UIUC ballast box, the first with the UBM sample placed on the bottom of the box over the flat steel bottom and a second with concrete tiles and no UBM to simulate installation on a concrete bridge deck. Neoprene sheets, one-quarter inch (6.35 mm) thick, were placed over the sidewalls, as specified by the DIN 45673-5, to provide elasticity to the ballast layer and better simulate particle confinement experienced in the field track conditions. Clean

ballast was added and compacted for 60 seconds in three 4-in. (10.2-cm) lifts; an adjustable formwork vibrator attached to a steel plate (Figure 4.3) provided a 1000-lbf (4.4-kN) compaction force at 60 Hz.

### 5.4.2 *Test Procedures*

DIN recommended load levels served as basis for the determination of the loads to be used during the testing procedures. The prescribed fatigue load levels 1 and 2 for the specific UBM stiffness used were 16.9 kips (75 kN) and 22.5 kips (100 kN), respectively representing the European loading scenario. These values were scaled based on the areas of the original plate design and UIUC loading plate to yield equivalent ballast stress levels of 38.5 psi (265 kPa) and 51.3 psi (354 kPa), respectively, as described in Section 2.2.2.1. Table 5.2 presents a summary of the load levels for the sinusoidal loading procedures.

**Table 5.2 Loading procedures employed**

| Loading Scenario | Load Level | Loading Range [kips (kN)] | | Sinusoidal Frequency [Hz] | No. of Cycles |
|---|---|---|---|---|---|
| | | Minimum | Maximum | | |
| European | Level 1 | 0.4 (1.8) | 4.4 (19.6) | 5 | $10x10^6$ |
| | Level 2 | 0.4 (1.8) | 5.8 (25.8) | 5 | $2.5x10^6$ |

The ballast box was placed in the testing frame. Displacements were measured using the four potentiometers equally spaced along the perimeter of the loading plate attached to the vertical actuator (Figure 5.3). Vertical transient displacement data were collected for ten consecutive cycles once every ten thousand cycles. Figure 5.4 presents the hysteresis loops representative of the system behavior under loading. After completion of 12.5 million loading cycles, the ballast material was carefully collected from the box and sieved for gradation check according to ASTM C136 (ASTM, 2014).

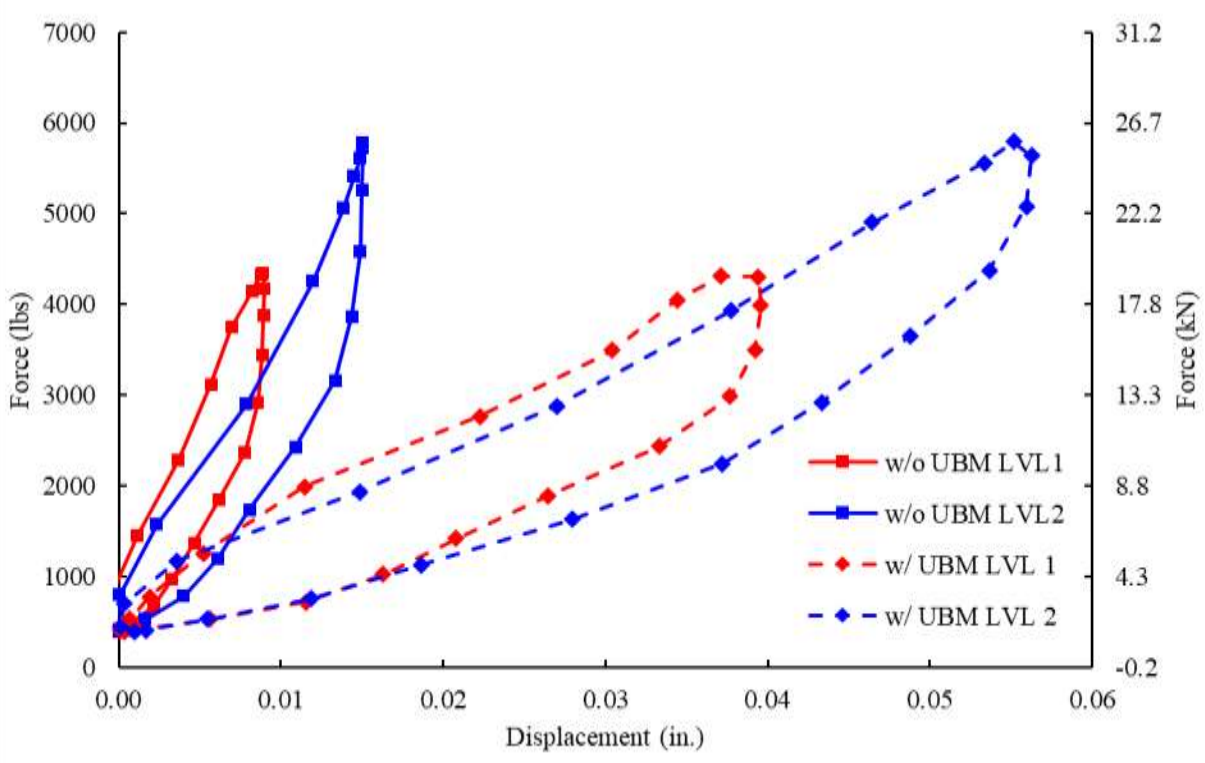


**Figure 5.4 Hysteresis loops applied to the system**

## 5.5 Results and Discussion

To account for possible tilting of the loading plate during the test, the analysis considered the average values obtained from the displacement data collected from all four potentiometers. Vertical transient deformation amplitudes were determined based on the maximum and minimum displacement values for every 10-cycle group collected. Figure 5.5 presents the results of this analysis. Sections of Figure 5.5 where amplitude results are omitted account for temporary instrumentation malfunction.

Ballast particle size distribution obtained after the test are presented in Figure 5.6 in comparison with the original gradation. The two gradations showed little variation. The most noticeable changes occurred in sieve sizes 1.5 and 1.0 in. (37.5 and 25.0 mm) with the largest difference being approximately 1.3 percent for the tests with UBM.

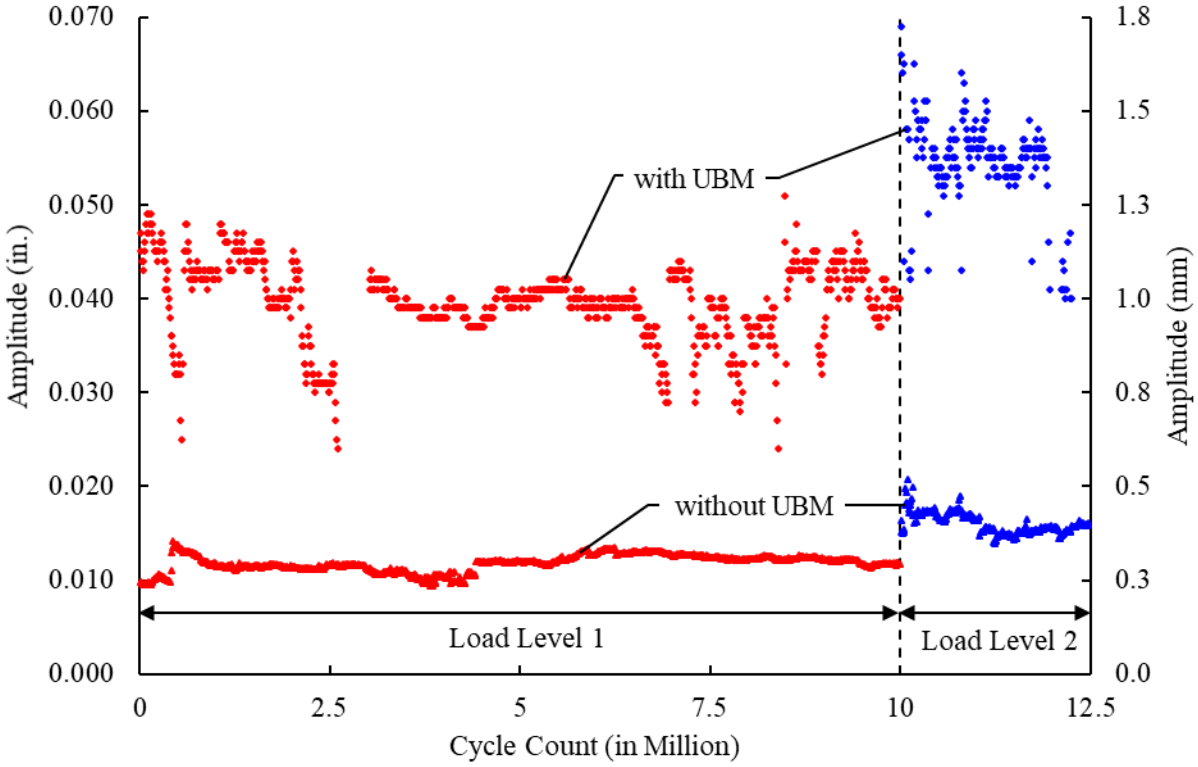


**Figure 5.5 Loading plate vertical movement amplitudes**

Visual assessment of the ballast after testing showed no noticeable particle breakage. This is also supported by particle size distributions as shown in Figure 5.6. Yet, fines that were not present in the clean original ballast were observed. The generation of additional fines in the ballast composition is believed to be due to relative movements between ballast particles as the system deforms under load, with large amplitudes of movement observed in the ballast surface as attested by Figure 5.5. Fines were generated as particle edges and corners chipped off, causing reductions in angularity, and the aggregate surfaces were subjected to frictional wear.

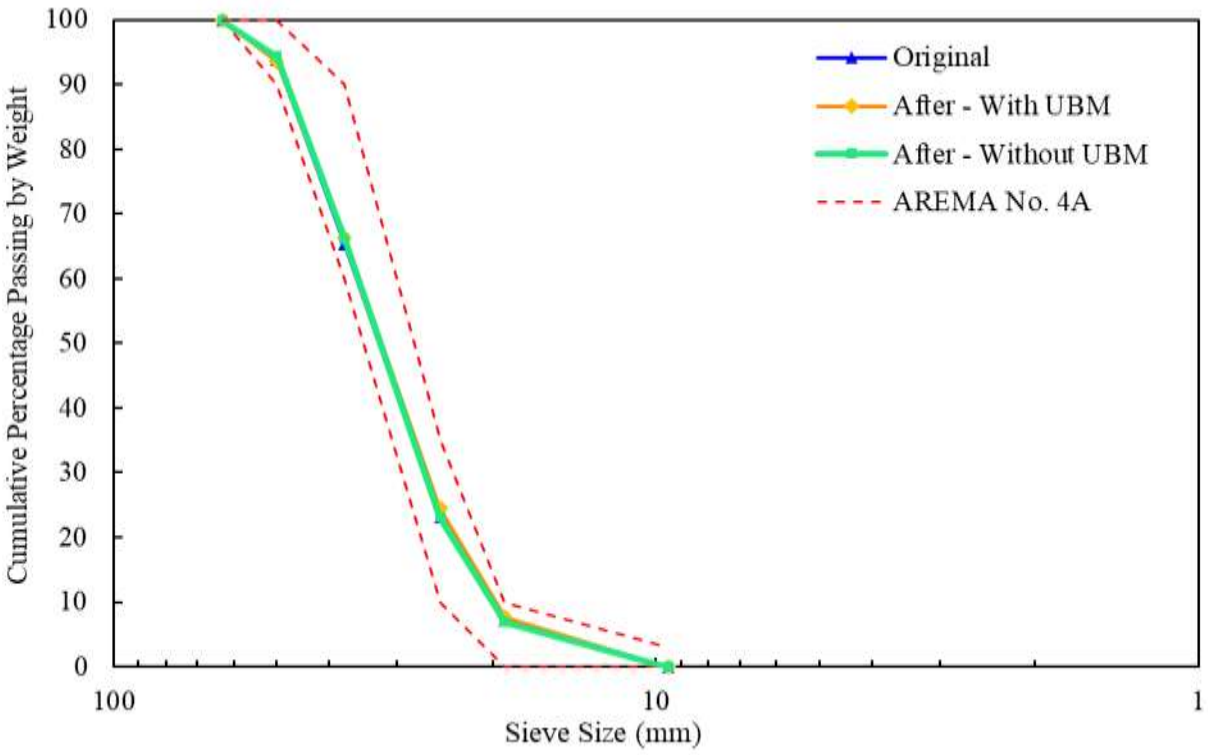


**Figure 5.6 Particle size distribution of the granite ballast material before and after testing**

The analyses of the results presented in Figure 5.5 show slight variations in the vertical system movement amplitudes. Tests conducted with the implementation of the concrete tiles served as a baseline value for the expected deflections over a rigid structure and provided average amplitudes of 0.013 in. (0.33 mm) and 0.018 in. (0.45 mm) for load levels 1 and 2, respectively. Whereas, for the test conducted with the UBM sample, values varied between 0.029-0.048 in. (0.70-1.20 mm) with an average of 0.040 in. (1.00 mm) obtained for load level 1. While for load level 2, values between 0.040-0.059 in. (1.00-1.50 mm) and an average of 0.054 in. (1.4 mm) were obtained. In fact, results showed an increase in amplitudes of 208% and 200% respectively for load levels 1 and 2. Moreover, during testing with an UBM sample installed, a clear vertical "bounce", or up-and-down movement, of the ballast surface could be observed as the entire composition moved with the application of every load cycle.

In an effort to compare the laboratory results, typical ranges of field obtained vertical transient deformations at track transition zones were gathered from the literature. There are various reports of field

monitoring of track transient deformations (Coelho et al. 2010, Mishra et al. 2012, Mishra et al. 2014, Stark & Wilk 2015, Varandas et al. 2011). Mishra et al. (2012) recorded deflections of various layers (ballast, subballast, subgrade, etc.) of the track substructure and observed a maximum total transient vertical deformation of approximately 0.066 in. (1.67 mm) from the bottom of the sleeper using a multidepth deflectometer (MDD). Mishra et al. (2014) and Stark & Wilk (2015) employed the same apparatus and reported approximate total substructure transient vertical deformations of 0.073 in. (1.85 mm), and 0.064 in. (1.62 mm), respectively. Interestingly, it is encouraging to observe that the UBM sample tested was able to provide ballast layer deflection values during testing comparable to the open track values measured in the field (Figure 5.7). These results provide evidence to the potential of UBMs to increase track elasticity over rigid substructures. Ultimately, this equalization of transient deformations could lead to the deceleration of the previously mentioned track degradation negative feedback loop in transition zones.

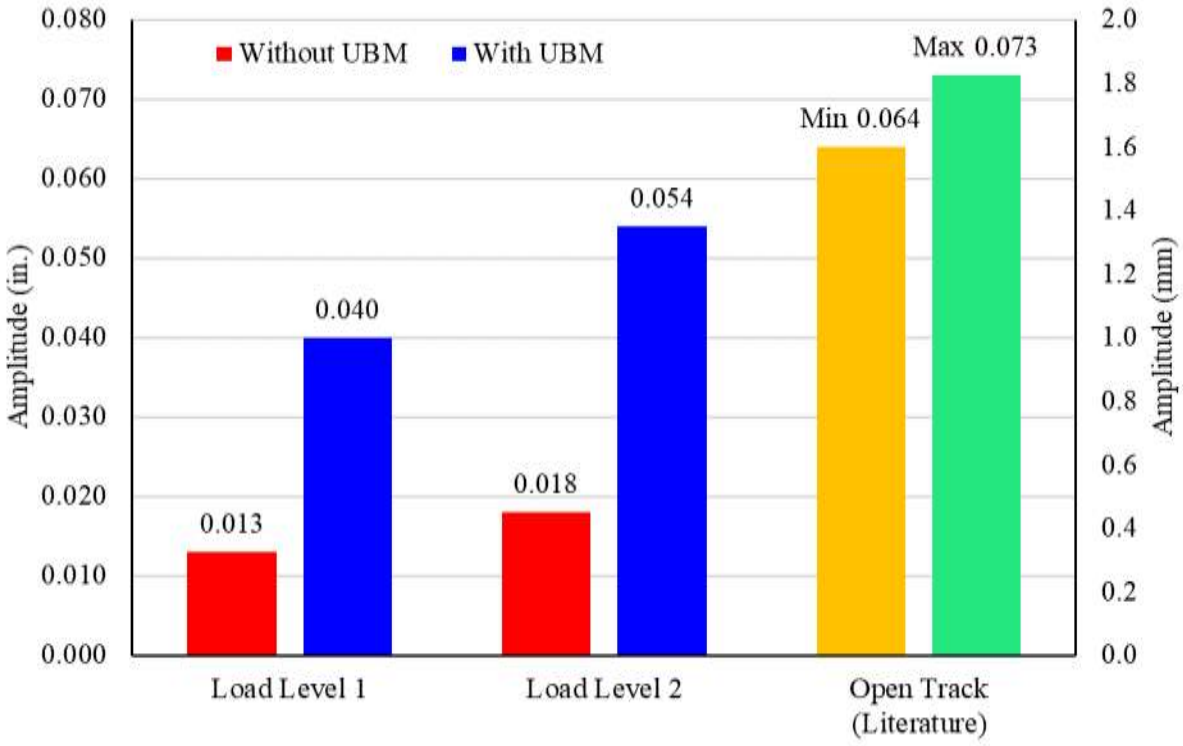


**Figure 5.7 Comparison between laboratory results and literature field measurements**

Note that the measurements obtained by Mishra et al. (2014) from the use of the MDDs represent the movement of the bottom of the sleeper and so, may include displacement due to gaps developed between the tie and the ballast layer (i.e. hanging ties) due to ballast migration and settlements. Additionally, it is necessary to emphasize the difficulty in replicating the exact field loading conditions in a laboratory setup. In field conditions, the tie/ballast contact is not always constant as the tie experiences uplifts between load applications (between axles). Consequently, there is a component of the measured displacements related to the deformation required before the ballast structure is mobilized, after which the true substructure deformations appear. Yet in the laboratory experiments - to maintain the stability of the servo-hydraulic system - a minimum load of 400 pounds (1.8 kN) was maintained throughout the entire duration of the test as recommended by DIN procedures. When evaluating Figure 5.4, note that the possible continuity of the hysteresis loop to zero load would provide additional measurements of displacement.

## 5.6 Conclusions

This chapter presented results from laboratory experiments aimed at evaluating and quantifying the overall fatigue performance of UBMs and their benefits to the life-cycle of ballast.

A test setup was developed based on recommended practices from the German DIN 45673-5 standard. An under ballast mat sample intended for freight applications was placed under a 12-in. (30.5-cm) ballast layer in a newly designed ballast box and subjected to 12.5 million repeated load applications. The employed ballast material was monitored for changes in particle size distribution, and vertical deformations of the system were collected in 10-cycle sections at regular 10,000-cycle intervals.

Test results from the sieve analysis conducted on the ballast material after completion of all loading cycles showed little signs of changes in gradation. Most of the observed deterioration was attributed to the relative movement between individual particles causing chipping off of sharp corners and

edges, and frictional wear. Visual assessments after testing, which demonstrated the presence of fines yet no noticeable particle breakage, supported this finding.

Average vertical transient deformation amplitudes recorded throughout testing were in the order of 0.040 in. (1.0 mm) for load level 1 and 0.054 in. (1.4 mm) for load level 2. Amplitudes monitored during testing were compared to field measured values reported in the literature. Such comparison showed that the 200 to 208 % increase in elasticity of the ballast structure due to the incorporation of the UBM resulted in movements was comparable to the field measurement values.

It is worth noting that, due to the explained differences in the tie/ballast contact between field and laboratory conditions, field results from transient deformations of track with UBMs installed in ballasted bridge decks could be larger than the laboratory obtained values, providing even closer transient deflection values to the ones obtained by field measurements.

# CHAPTER 6: CONCLUSIONS AND FUTURE WORK

This thesis presented work conducted to better understand the behavior and performance of under ballast mat (UBM) components for railway track. Concurrently, it investigated the impacts of changes to current standardized European test practices to both streamline testing and better represent N.A. HAL service conditions. A variety of test procedures and conditions were evaluated throughout this thesis in five main chapters.

First, Chapter 1 presented a literature review introducing UBMs, including current uses and benefits, and documented the available standard test practices worldwide. Following, Chapter 2 provided a summary of the equipment and basic testing procedures used in the subsequent chapters. Laboratory experiments described in Chapter 3 aimed to investigate the effects of varying support conditions, loading procedures, and sample conditioning to the UBM's bedding modulus values and resulting insertion loss estimations. Further, Chapter 4 presented results from mechanical fatigue tests conducted to compare two different fatigue test setups (i.e. ballast box and geometric ballast plate). Lastly, Chapter 5 provided insights into UBMs ability to reduce stiffness and increase transient deformations to mitigate accelerated degradation rates common at transition zones.

## 6.1 Summary of Findings

### 6.1.1 *The effects of varying loads and support conditions to the bedding modulus and insertion loss of under ballast mats (Chapter 3)*

Laboratory methods used for the determination of static bedding modulus of under ballast mat samples exhibited high levels of repeatability (< 3.8% from the mean) for all support conditions tested. Yet, tests conducted with the steel support yielded the most consistent results. The uniformity of the steel – in terms of surface irregularities – is believed to be the main factor affecting this result. The same mechanism (i.e. friction at the sample-support interface) has been hypothesized to produce consistently larger bedding modulus results for the concrete support versus steel. Overall, results found the GBP

support condition to yield the lowest bedding moduli with values up to 33.3% lower than the other two support conditions tested. Additionally, statistical analyses of the results concluded that there were significant differences among all the three support conditions tested. Nevertheless, results obtained with the GBP setup provided the means to a proposed adoption of this apparatus for testing of UBMs, both for bedding modulus and fatigue resistance determinations.

Static bedding modulus values obtained from all support conditions were used to quantify the effects of variations in bedding modulus inputs to the estimated insertion loss performance based on analytical prediction models from the literature. Resulting insertion loss calculations from the various support conditions showed average variations of up to 1.8 dB; a value which can be significant depending on the mitigation level required for a specific project. This finding highlighted the need for bedding modulus to be representative of its proposed application environment so that component performance may be correctly predicted.

Further, results from the three simulation procedures performed on the samples (i.e. preload conditioning, continuous loading stiffening, and stiffening and recovery) provided insights into the changes in sample stiffness characteristics due to loading and/or rest patterns. First, preload conditioning tests demonstrated the rapid development of preconditioning stiffening due to a constant static load while stiffening magnitudes were found to be constant and independent of load duration. Secondly, continuous loading stiffening results showed bedding modulus values to gradually increase with the accumulation of loading cycles by the sample. Further, high rates of elastic recovery development were observed during the rest phase of the tests. Third, the proposed "working range" of bedding modulus values could be observed in the stiffening and recovery test scenario where samples reached an asymptote range with no observable effects of traffic density. Undoubtedly, all results obtained provided valuable insights to the development of new representative test procedures to assess UBM characteristics and performance for N.A applications.

### 6.1.2 *Comparison between the fatigue performance of under ballast mats using a ballast box and a geometric ballast plate under increased loading conditions (Chapter 4)*

Similar fatigue performance results were observed from the two employed test setups. During fatigue performance assessments, under ballast mat samples demonstrated good capacity to withstand the loading imparted in all test configurations. Physical deterioration was minimal and only noticeable in samples tested under the simulated N.A. loading conditions. Minor cracks and/or tears were present around the edges of contact points with ballast particles or plate indents and were superficial only and so believed not to deteriorate the performance of the components. Also, imprint deformations at the same contact points were observed in the N.A. samples directly after testing, only partially recovering after rest. All the above observations evidenced the difference in component behavior with the employment of higher loads representative of N.A. HAL and so attest to the importance of considering representative loading conditions to evaluate component performance for specific applications.

Differences between the two test setups were more noticeable in the evaluation of bedding modulus changes due to the imparted fatigue loading. Results from ballast box tests demonstrated a considerable increase in bedding modulus immediately after the tests under N.A. loading conditions (67%). Yet, these values were reduced to only 8% after the sample could rest for a one-week period. A similar behavior, but in much smaller scale, was observed for the European sample as well. Since the tests simulated continuous loading of the system for the totality of cycles prescribed, the values obtained after rest are believed to better represent the true component behavior under intermittent traffic loading. Small differences in behavior are observed when comparing bedding modulus change results between the two test setups – using after-rest results from ballast box. Differences found – 8% vs. -3% and 9% vs. 5%/11% for European and N.A. tests respectively – are believed to be mostly related to test/sample variability, hence leading researchers to conclude the geometric ballast plate to be an effective alternative method to assessing the mechanical fatigue performance of UBM samples.

Finally, effects of UBMs on ballast material degradation trends were investigated during tests conducted in the ballast box setup. Results showed no signs of particle breakage and minor changes in

particle size distribution of the material collected. Changes were attributed to the generation of fines due to wear as a result of relative movements of particles in the system.

### 6.1.3 *Improvement of differential movements in transition zones using under ballast mats (Chapter 5)*

Particle size distribution of the ballast material employed in the box tests demonstrated little signs of deterioration in the ballast material after completion of 12.5 million loading cycles independent of test condition (i.e. with or without an under ballast mat). Most of the deterioration is believed to have occurred due to particle-to-particle interactions resulting in sharp corners and edges chipping off, and surface frictional wear. The presence of fines during final collection of the ballast material combined with small size reduction shifts observed in the gradation curves of both tests conducted supported this understanding.

Furthermore, measurements of system deflection amplitudes during tests demonstrated that under ballast mats can increase the average deflections of a rigid system (i.e. ballast over rigid structure) by up to 208%. Average deflection values measured were of 0.040 in. (1.0 mm) and 0.054 in. (1.4 mm) for the two load levels employed, respectively. Results are encouraging when compared to literature-obtained field measurements on bridge approaches with deflection amplitudes between 0.064 in. (1.62 mm) and 0.073 in. (1.85 mm) (Mishra et al., 2012; Mishra et al., 2014; Stark and Wilk, 2016) as differential movements are large contributors to the negative feedback loop of track quality degradation.

### 6.1.4 *Summary*

Research described in this thesis had an overarching objective of providing a better understanding of current testing procedures and how each of its components (e.g. loading, support, cycles, etc.) could influence the behavior of under ballast mat components. Ultimately, results presented in this work are intended to assist in the development of suitable testing procedures to evaluate the performance of UBMs for applications in N.A railway tracks. Therefore, in summary, this thesis:

- Demonstrated the importance of considering representative loading and support characteristics for evaluating UBM's performance metrics;
- Attested to UBM's capability of withstanding N.A. HAL loading conditions;
- Validated the use of simplified mechanical fatigue testing using the GBP;
- Presented findings related to UBM's effectiveness in improving transient deformation of rigid track structures.

## 6.2 Recommendations and Future Work

Results presented in this thesis are part of an ongoing research effort at UIUC to understand and characterize the behavior of resilient components for railway track. To this extent, parallel work is currently ongoing to investigate similar aspects of under-sleeper pad (USP) testing procedures based on the knowledge from the work presented in this document.

With the consistent growth in the adoption of resilient components (i.e. UBM and USP) in N.A railways, the rapid development of testing procedures suitable to such applications is critical. As such, efforts are ongoing within AREMA Committee 30 (Ties) to develop and/or adopt modified versions of the already established tests available in Europe (an EN norm is rumored to be released within calendar year 2018). Based on findings from this research, modifications to be considered are:

- Load range magnitudes for each intended application;
- Method of sample preconditioning;
- Total number of cycles for mechanical fatigue tests; and
- Use of the geometric ballast plate for mechanical fatigue tests.

Further, different methods of quantifying the performance of resilient components could be investigated. The energy absorption (e.g. entropy) of the component during dynamic fatigue loading may be quantified for predetermined cycle intervals to elaborate on the gradual change in component

performance due to cyclic loading – for this, the use of the GBP setup must be considered to allow reliable measurements. In addition, the redistribution of stresses in the track structure due to the inclusion of UBMs should be investigated both in the ballast structure and in the ballast-support interface.

## REFERENCES


American Association of State Highway and Transportation Officials (AASHTO). 2011. *Reducing Sample of Aggregate to Testing Size*, T-258. American Association of State Highway and Transportation Officials, Washington, DC, USA.

Alves Costa, P., R. Calçada and A. Silva Cardoso. 2012. Ballast mats for the reduction of railway traffic vibrations – Numerical study. *Soil Dynamics and Earthquake Engineering*, 42: 137–150.

American Railway Engineering and Maintenance-of-Way Association (AREMA). 2012. *Manual for Railway Engineering*. The American Railway Engineering and Maintenance-of-Way Association, Landover, MD, USA.

Association of American Railroads (AAR). 2016. *Total Annual Spending - 2015 Data*. Association of American Railroads, Washington, DC, USA.

ASTM International. 2014. *Standard Test Method for Sieve Analysis of Fine and Coarse Aggregates*, C136. ASTM International, West Conshohocken, PA.

Auersch, L. 2006. Dynamic Axle Loads on Tracks With and Without Ballast Mats: Numerical Results of Three-Dimensional Vehicle-Track-Soil Models. *Proceedings of the Institution of Mechanical Engineers, Part F: Journal of Rail and Rapid Transit*, 220(2): 169–183.

Banimahd, M., P. Woodward, J. Kennedy and G.M. Medero. 2012. Behavior of Train-Track Interaction in Stiffness Transition. *Proceedings of the Institution of Civil Engineers - Transport*, 165(3): 205–214.

Bauman, J.T. 2008. *Fatigue, Stress, and Strain of Rubber Components: A Guide for Design Engineers*. Hanser Publications, Cincinnati, OH, USA.

Briaud, J., J.E. Nicks and B. Smith. 2006. *The Bump at The End of the Railway Bridge*. Texas A&M Transportation Institute, College Station, TX, USA.

British Standard Institution. 2016. *Railway Applications - Track - Concrete Sleepers and Bearers With Under Sleeper Pads*, BS EN 16730. British Standards Institution, London, UK.

Coelho, B., P. Hölscher, J. Priest, W. Powrie and F. Barends. 2011. An Assessment of Transition Zone Performance. *Proceedings of the Institution of Mechanical Engineers, Part F: Journal of Rail and Rapid Transit*, 225(2): 129–139.

Dahlberg, T. 2003. *Railway Track Settlements – A Literature Review*, Report for the EU project SUPERTRACK, Linkoping University, Linkoping, Sweden.

Dahlberg, T. 2010. Railway Track Stiffness Variations – Consequences and Countermeasures. *International Journal of Civil Engineering*, 8(1): 1–12.

Deutsches Institut fur Normung. 2010a. *Mechanical Vibration - Resilient Elements Used in Railway Tracks - Part 1: Terms and Definitions, Classification, Test Procedures,* DIN 45673-1. Deutsches Institut fur Normung, Berlin, Germany.

Deutsches Institut fur Normung. 2010b. *Mechanical Vibration - Resilient Elements Used in Railway Tracks - Part 5: Laboratory Test Procedures for Under-Ballast Mats,* DIN 45673-5. Deutsches Institut fur Normung, Berlin, Germany.

Dold, M. and S. Potocan. 2013. Long-term Behaviour of Sylomer Ballast Mats. *Rail Technology Review*, 53.

European Rail Research Institute (ERRI). 1999. *State of The Art Report – Bridge Ends Embankment Structure Interaction*. European Rail Research Institute, Netherlands.

Esveld, C. 2001. *Modern Railway Track*, 2nd ed. MRT-Productions, Zaltbommel, Netherlands.

Frohling, R.D., H. Sheffel and W. Ebersohn. 2005. The Vertical Dynamic Response of a Rail Vehicle Caused by Vertical Stiffness Variations Along the Track. In: *Proceedings of the 14th IAVSD Symposium*, Prague, Czech Republic.

Giannakos, K. 2010a. Loads on Track, Ballast Fouling, and Life Cycle Under Dynamic Loading in Railways. *Journal of Transportation Engineering*, 136(12): 1075–1084.

Giannakos, K. 2010b. Stress on Ballast-Bed and Deterioration of Geometry in a Railway Track. *Journal of Civil Engineering and Architecture*, 4(6): 31.

Hanson, C., D.A. Towers and L.D. Meister. 2006. *Transit Noise and Vibration Impact Assessment*. US Department of Transportation, Federal Transit Administration FTA-VA-90-1003-06, Washington, DC, USA.

Hanson, C.E. and H.L. Singleton. 2006. Performance of Ballast Mats on Passenger Railroads: Measurement vs. Projections. *Journal of Sound and Vibration*, 293(3–5): 873–877.

Hay, W.W. 1982. *Railroad Engineering*, 2nd ed. John Wiley & Sons, New York, NY, USA.

Hopkinson, B. and G.T. Williams. 1912. The Elastic Hysteresis of Steel. *Proceedings of the Royal Society of London A: Mathematical, Physical and Engineering Sciences*, 87(598): 502–511.

Hunt, H. 1997. Settlement of railway track near bridge abutments. *Proceedings of the Institution of Civil Engineers - Transport*, 123(1).

Hussein, M.F.M. 2004. *Vibration from Underground Railways*. Doctoral Thesis. University of Cambridge, Engineering Department, Cambridge, UK.

Hyslip, J., D. Li and C. McDaniel. 2009. *Railway Bridge Transition Case Study*. In: Proceedings of the 8th International Conference on Bearing Capacity of Roads, Railways and Airfields, Champaign, IL, USA.

Indraratna, B. 2016. 1st Ralph Proctor Lecture of ISSMGE: Railroad Performance with Special Reference to Ballast and Substructure Characteristics. *Transportation Geotechnics*, 7: 74–114.

Indraratna, B., S. Nimbalkar, S.K. Navaratnarajah, C. Rujikiatkamjorn and T. Neville. 2014. Use of Shock Mats for Mitigating Degradation of Railroad Ballast. *Special Issue on Ground Improvement - Sri Lankan Geotechnical Society International Conference*, 6(1): 32–41.

International Union of Railways (UIC). 2011. *State of The Art Review of Mitigation Measures on Track*, RIVAS_UIC_ WP3_D3_1_V01-3. International Union of Railways, Paris, France.

Jenks, C.W. 2006. *Design of Track Transportations*. US Department of Transportation, Federal Railroad Administration Research Results Digest 79, Washington, DC, USA.

Jones, C.J.C. and J.R. Block. 1996. Prediction of Ground Vibration from Freight Trains. *Journal of Sound and Vibration*, 193(1): 205–213.

Kerr, A.D. 2003. *Fundamentals of Railway Track Engineering*, 1st ed. Simmons-Boardman Books, Omaha, NE, USA.

Kerr, A.D. and B.E. Moroney. 1993. Track Transition Problems and Remedies. In: *Proceedings of The American Railway Engineering Association*, 267–298.

Le Pen, L.M. and W. Powrie. 2011. Contribution of Base, Crib, and Shoulder Ballast to the Lateral Sliding Resistance of Railway Track: A Geotechnical Perspective. *Proceedings of the Institution of Mechanical Engineers, Part F: Journal of Rail and Rapid Transit*, 225 (2): 113–128.

Li, D. and D. Davis. 2005. Transition of Railroad Bridge Approaches. *Journal of Geotechnical Engineering*, 131(11): 1392–1398.

Li, D. and L. Maal. 2015. Heavy Axle Load Revenue Service Bridge Approach Problems and Remedies. In: *Proceedings of the 2015 Joint Rail Conference*, American Society of Mechanical Engineers, San Jose, CA, USA.

Lima, A. de O., M.S. Dersch, Y. Qian, E. Tutumluer and J.R. Edwards. 2017a. Laboratory Evaluation of Under-Ballast Mat Effectiveness to Mitigate Differential Movement Problem in Railway Transition Zones. In: *Proceedings of the 10th International Conference on Bearing Capacity of Roads, Railways and Airfields*, Athens, Greece.

Lima, A. de O., M.S. Dersch, Y. Qian, E. Tutumluer and J.R. Edwards. 2017b. Laboratory Mechanical Fatigue Performance of Under-Ballast Mats Subjected to North American Loading Conditions. In*: Proceedings of the 11th International Heavy Haul Association Conference*, Cape Town, South Africa.

Lu, M. and G. McDowell. 2010. Discrete Element Modelling of Railway Ballast Under Monotonic and Cyclic Triaxial Loading. *Geotechnique*, 60(6): 459–467.

Lundqvist, A., R. Larsson and T. Dahlberg. 2006. Influence of railway track stiffness variations on wheel/rail contact force. In: *Track for High Speed Railways*, Porto, Portugal.

Mademann, C. and D. Otter. 2013. *Summary of Stress-State Reduction in Concrete Bridges*. AAR Research Report TD-13-025, Transportation Technology Center, Inc., Pueblo, CO, USA.

Mars, W.V. and A. Fatemi. 2004. Factors That Affect the Fatigue Life of Rubber: A Literature Survey. *Rubber Chemistry and Technology*, 77(3): 391–412.

Marschnig, S. and P. Veit. 2011. Making a Case for Under-Sleeper Pads. *International Railway Journal*, 51(1): 27–29.

Mishra, D., E. Tutumluer, H. Boler, J.P. Hyslip and T.R. Sussmann Jr. 2014. Railroad Track Transitions with Multidepth Deflectometers and Strain Gauges. *Transportation Research Record: Journal of the Transportation Research Board*, 2448: 105–114.

Mishra, D., E. Tutumluer, T.D. Stark, J.P. Hyslip, S.M. Chrismer and M. Tomas. 2012. Investigation of differential movement at railroad bridge approaches through geotechnical instrumentation. *Journal of Zhejiang University SCIENCE A*, 13(11): 814–824.

Müller, G. & M. Möser. 2013. *Handbook of Engineering Acoustics*. Springer-Verlag Berlin Heidelberg, Berlin, Germany.

Müller, R. 2008. Mitigation Measures for Open Lines Against Vibration and Ground-Borne Noise: A Swiss Overview. *Noise and Vibration Mitigation for Rail Transportation Systems*, pp. 264–270.

Nicks, J.E. 2009. *The Bump at the End of The Railway Bridge*. Doctoral Thesis, Texas A&M University, College Station, TX, USA.

Nimbalkar, S., B. Indraratna, S.K. Dash and D. Christie. 2012. Improved Performance of Railway Ballast under Impact Loads Using Shock Mats. *Journal of Geotechnical and Geoenvironmental Engineering*, 138(3): 281–294.

Nunez, J. 2014. Gripping Fastening Systems. *Railway Track and Structures*, July, pp. 14–18.

Qian, Y., H. Boler, M. Moaveni, E. Tutumluer, Y. Hashash and J. Ghaboussi. 2014. Characterizing Ballast Degradation Through Los Angeles Abrasion Test and Image Analysis. *Transportation Research Record: Journal of the Transportation Research Board*, 2448: 142–151.

Roberts, R., J. Rudy, I. Al-Qadi, E. Tutumluer and J. Boyle. 2006. Railroad Ballast Fouling Detection Using Ground Penetrating Radar – A New Approach Based on Scattering from Voids. In: *Proceedings of The Ninth European Conference On NDT*, Berlin, Germany.

Schilder, R. 2013. USP (Under Sleeper Pads): A Contribution to Save Money in Track Maintenance. In: *AusRAIL PLUS*, Canberra, Australia.

Sasaoka, C.D. and D. Davis. 2005. Implementing Track Transition Solutions for Heavy Axle Load Service. In: *Proceedings of the 2005 American Railway Engineering and Maintenance-of-Way Association Annual Conference*, Chicago, IL, USA.

Sato, Y. and T. Usami. 1976. Test Results of Various Types of Ballast-Mat and Characteristics of A45 Ballast-Mat. *Quarterly Reports of the Railway Technical Research Institute Vol. 18 No. 2*. Tokyo, Japan.

Sato, Y., T. Usami and Y. Satoh. 1974. Development of Ballast-Mat. *Quarterly Reports of the Railway Technical Research Institute Vol. 15 No. 3*. Tokyo, Japan.

Sawadisavi, S.V. 2010. Development of Machine-Vision Technology for Inspection of Railroad Track. Master's Thesis, University of Illinois at Urbana-Champaign, Department of Civil and Environmental Engineering, Urbana, IL, USA.

Selig, E.T., B.I. Collingwood and S.W. Field. 1988. Causes of fouling in track. *AREA Bulletin 717*, Washington, DC, USA.

Selig, E.T. and J.M. Waters. 1994. *Track Geotechnology and Substructure Management*. Thomas Telford, London, UK.

Sol-Sánchez, M., F. Moreno-Navarro and M. Rubio-Gámez. 2015. The Use of Elastic Elements in Railway Tracks: A State of the Art Review. *Construction and Building Materials*, 75: 293–305.

Sol-Sánchez, M., F. Moreno-Navarro and M.C. Rubio-Gámez. 2014. The Use of Deconstructed Tires as Elastic Elements in Railway Tracks. *Materials*, 7(8): 5903–5919.

Stahl, W. 2016. Question and Request for Assistance: Ballast Loading Plate (DIN 45673). *Personal Communication, 5 May.*

Stark, T.D. and S.T. Wilk. 2016. Root Cause of Differential Movement at Bridge Transition Zones. *Proceedings of the Institution of Mechanical Engineers, Part F: Journal of Rail and Rapid Transit*, 230(4): 1257–1269.

Talbot A. N. 1920. *Second progress report: Special committee on stresses in railroad track*. American Railway Engineering Association, Washington, DC, USA.

T. J. LaClair. 2006. *The Pneumatic Tire – Chapter 11 Rolling Resistance*. US Department of Transportation National Highway Traffic Safety Administration DOT HS 810 561, Washington, DC, USA.

Thompson, D. 2008. *Railway Noise and Vibration: Mechanisms, Modelling and Means of Control*. Elsevier, Amsterdam, The Netherlands.

Tutumluer, E. and T. Pan. 2008. Aggregate Morphology Affecting Strength and Permanent Deformation Behavior of Unbound Aggregate Materials. *Journal of Materials in Civil Engineering*, 20(9): 617–627.

Tutumluer, E., T.D. Stark, D. Mishra and J.P. Hyslip. 2012. Investigation and Mitigation of Differential Movement at Railway Transitions for US High Speed Passenger Rail and Joint Passenger/Freight Corridors. In: *Proceedings of the 2012 Joint Rail Conference*, American Society of Mechanical Engineers, Philadelphia, PA, USA.

Van Dyk, B. 2013. Characterization of the Loading Environment for Shared-Use Railroad Superstructure in North America. Master's Thesis, University of Illinois at Urbana-Champaign, Department of Civil and Environmental Engineering, Urbana, IL, USA.

Varandas, J.N., P. Hölscher and M.A.G. Silva. 2011. Dynamic Behaviour of Railway Tracks on Transitions Zones. *Computers & Structures*, 89(13–14): 1468–1479.

Vuchic, V.R. 2007. *Urban Transit Systems and Technology*. John Wiley & Sons, Hoboken, NJ, USA.

Wang, B., U. Martin and S. Rapp. 2017. Discrete Element Modeling of the Single-Particle Crushing Test for Ballast Stones. *Computers and Geotechnics*, 88: 61–73.

Wang, H., V.L. Markine, I.Y. Shevtsov and R. Dollevoet. 2015. Analysis of the Dynamic Behaviour of a Railway Track in Transition Zones with Differential Settlement. In: *Proceedings of the 2015 Joint Rail Conference*, American Society of Mechanical Engineers, San Jose, CA, USA.

Wettschureck, G., M. Heim and M. Tecklenburg. 2002. Long-term Properties of Sylomer® Ballast Mats Installed in the Rapid Transit Railway Tunnel Near the Philharmonic Hall of Munich, Germany. *Rail Engineering International*, 31(4): 6–11.

Wettschureck, R. 1997. Measures to Reduce Structure-Borne Noise Emissions Induced by Above-Ground, Open Railway Lines. *Rail Engineering International*, 1: 12–16.

Wettschureck, R. and U.J. Kurze. 1985. Insertion Loss of Ballast Mats. *Acustica*, 58(3): 177–182.

Wettschureck, R.G. 1994. Vibration and Structure-Borne Sound Isolation by Means of Cellular Polyurethane (PUR) Elastomers. *Swedish Vibration Society*, Stockholm, Sweden.

Wettschureck, R.G., F. Breuer, M. Tecklenburg and H. Widmann. 1999. Installation of Highly Effective Vibration Mitigation Measures in a Railway Tunnel in Cologne, Germany. *Rail Engineering International*, Edition 1999 (4): 12–16.

Wettschureck, R.G., M. Heim and M. Tecklenburg. 2003. Long-Term Efficiency of Ballast Mats Installed in the Rapid Transit Railway Tunnel near the Philharmonic Hall of Munich Germany. In: *Proceedings of the Tenth International Congress on Sound and Vibration*, 403–410.

Wilson, G.P., H.J. Saurenman and J.T. Nelson. 1983. Control of Ground-Borne Noise and Vibration. *Journal of Sound and Vibration*, 87(2): 339–350.

Wnek, M., E. Tutumluer, M. Moaveni and E. Gehringer. 2013. Investigation of Aggregate Properties Influencing Railroad Ballast Performance. *Transportation Research Record: Journal of the Transportation Research Board*, 2374: 180–189.

Woo, C.S. and H.S. Park. 2011. Useful Lifetime Prediction of Rubber Component. *Engineering Failure Analysis*, 18(7): 1645–1651.

Woodward, P., P. Boyd and M. Banimahd. 2007. XiTRACK Reinforcement of Tunnel Railway Tracks from Floating to Fixed Geometry in a Day. In: *Proceedings of the 9th International Conference on Railway Engineering*, London, UK.

Zarembski, A. 1993. *Tracking R&D, Research & Development*, 1st ed. Simmons-Boardman Books, Omaha, NE, USA.